



This is a repository copy of *Spatially controlled occlusion of polymer-stabilized gold nanoparticles within ZnO*.

White Rose Research Online URL for this paper:
<https://eprints.whiterose.ac.uk/143119/>

Version: Accepted Version

Article:

Ning, Y. orcid.org/0000-0003-1808-3513, Fielding, L.A., Nutter, J. et al. (3 more authors) (2019) Spatially controlled occlusion of polymer-stabilized gold nanoparticles within ZnO. *Angewandte Chemie International Edition*, 58 (13). pp. 4302-4307. ISSN 1433-7851

<https://doi.org/10.1002/anie.201814492>

This is the peer reviewed version of the following article: Ning, Y. , Fielding, L. A., Nutter, J. , Kulak, A. N., Meldrum, F. C. and Armes, S. P. (2019), Spatially Controlled Occlusion of Polymer-Stabilized Gold Nanoparticles within ZnO. *Angew. Chem. Int. Ed.*, which has been published in final form at <https://doi.org/10.1002/anie.201814492>. This article may be used for non-commercial purposes in accordance with Wiley Terms and Conditions for Use of Self-Archived Versions.

Reuse

Items deposited in White Rose Research Online are protected by copyright, with all rights reserved unless indicated otherwise. They may be downloaded and/or printed for private study, or other acts as permitted by national copyright laws. The publisher or other rights holders may allow further reproduction and re-use of the full text version. This is indicated by the licence information on the White Rose Research Online record for the item.

Takedown

If you consider content in White Rose Research Online to be in breach of UK law, please notify us by emailing eprints@whiterose.ac.uk including the URL of the record and the reason for the withdrawal request.



eprints@whiterose.ac.uk
<https://eprints.whiterose.ac.uk/>

Angewandte Chemie

Spatially-Controlled Occlusion of Polymer-Stabilized Gold Nanoparticles within ZnO --Manuscript Draft--

Manuscript Number:	
Article Type:	Communication
Corresponding Author:	Steven Peter Armes, Prof. University of Sheffield Sheffield, UNITED KINGDOM
Corresponding Author E-Mail:	S.P.Armes@sheffield.ac.uk
Order of Authors (with Contributor Roles):	Steven Peter Armes, Prof. Yin Ning Lee Fielding Alexander Kulak Fiona Meldrum
Keywords:	spatially-controlled occlusion; metal/semiconductor nanocomposites; gold nanoparticles; ZnO; RAFT polymerization.
Manuscript Classifications:	Colloids; Nanocomposites; Nanoparticles; Nanotechnology; Polymers
Suggested Reviewers:	<p>Stephen Mann s.mann@bristol.ac.uk Prof. S. Mann is an internationally recognized expert in biomineralization.</p> <p>Lara Estroff lae37@cornell.edu Prof. Estroff has worked extensively on incorporating polymer gel networks into inorganic crystals.</p> <p>James De Yoreo jjdy@uw.edu Prof. De Yoreo is an internationally-recognised expert in biomineralization and nanoparticle occlusion mechanisms</p> <p>Han Li hanying_li@zju.edu.cn Prof. Li has worked on the incorporation of nanoparticles (such as Au, Fe₃O₄ and quantum dots) into calcite single crystals. His expertise is closely related to our research area.</p> <p>Dong Kim dhkim@ewha.ac.kr Prof. Kim has worked on Au/ZnO nanocomposite crystals</p>
Opposed Reviewers:	
Abstract:	<p>In principle, incorporating nanoparticles into growing crystals offers an attractive and highly convenient route for the production of a wide range of novel nanocomposites. Herein we describe an efficient aqueous route that enables the spatially-controlled occlusion of gold nanoparticles (AuNPs) within growing ZnO crystals at up to 20 % by mass. Depending on the precise synthesis protocol, these AuNPs can be (i) solely located within a central region, (ii) uniformly distributed throughout the ZnO host crystal or (iii) confined to a surface layer. Remarkably, such efficient occlusion is mediated by a non-ionic water-soluble polymer, poly(glycerol monomethacrylate)₇₀ (G70), which is chemically grafted to the AuNPs; pendant cis-diol side-groups on this steric stabilizer bind Zn²⁺ cations, which promotes nanoparticle interaction with the growing ZnO crystals. Finally, uniform occlusion of G70-AuNPs within this inorganic host leads to faster UV-induced photodegradation of a model dye.</p>
Author Comments:	Dear Prof. Compton,

We request that the attached manuscript entitled "Spatially-controlled Occlusion of Polymer-stabilized Gold Nanoparticles within ZnO" by Yin Ning, Lee A. Fielding, Alexander N. Kulak, Fiona C. Meldrum and Steven P. Armes is considered for publication in Angewandte Chemie International Edition.

Justification for Publication. Occlusion of polymeric nanoparticles within calcite crystals is of significant recent interest (see Y. Y. Kim, S. P. Armes, F. C. Meldrum et al., Nat. Mater. 2011, 10, 890; K. R. Cho, S. P. Armes, F. C. Meldrum, J. J. Yoreo et al., Nat. Commun. 2016, 7, 10187; Y. Ning, F. C. Meldrum, S. P. Armes et al., J. Am. Chem. Soc. 2016, 138, 11734.). This is because incorporating nanoparticles into growing crystals offers an attractive and highly convenient route to a wide range of novel nanocomposites. However, precise control over the spatial distribution of the guest nanoparticles within the host crystals remains a formidable technical challenge. The novelty of the present study is summarized by the following six points.

1. We report for the first time a simple yet efficient protocol for the incorporation of gold nanoparticles (AuNPs) at remarkably high levels (~20 % w/w) into a semiconductor host crystal (ZnO) during in situ crystallization of the latter phase in aqueous media.

2. For successful occlusion, the AuNPs were surface-modified using poly(glycerol monomethacrylate)70 (G70): we show that the G70 chains bind to Zn²⁺ and hence play an active role in AuNP occlusion within the ZnO.

3. This is a very rare example of a non-ionic polymeric stabilizer being used to promote efficient occlusion of nanoparticles in host crystals - almost all other literature examples require the use of anionic polymers.

4. We demonstrate exquisite control over the spatial localization of G70-AuNPs within ZnO. In particular, we prepare three types of nanocomposite crystals: (i) G70-AuNPs localized mainly in the central region of rod-like ZnO crystals, (ii) uniform occlusion of G70-AuNPs throughout the host crystals, or (iii) G70-AuNPs occluded solely within a 35 nm surface layer. Such fine control provides an unprecedented opportunity to elucidate synthesis-structure-property relationships.

5. We show that incorporation of AuNPs throughout the whole ZnO crystal leads to enhanced photocatalytic performance, as judged by the UV-induced decomposition of a model dye (rhodamine B).

6. Moreover, appropriate surface modification should enable our approach to be extended to include other metal nanoparticles, hence providing access to a wide range of new functional nanocomposite materials. We have preliminary data to support this hypothesis, although this is not included in the present study.

We are confident that this study will be of interest to a wide range of academics, including colloid scientists, polymer chemists, inorganic chemists, materials scientists, supramolecular chemists and all those working in the general area of nanoparticles and nanotechnology. Thus we seek rapid publication in a high-profile journal with a broad readership.

We look forward to hearing from you in due course.

N.B, The submitted version manuscript contains multiple colour Figures to facilitate the reviewers, but we intend to use black & white Figures for the final version of this manuscript (if it is accepted for publication).

Yours sincerely,

Prof. Steven P. Armes FRS and Dr. Yin Ning (on behalf of all of the co-authors)

Section/Category:

Additional Information:

Question

Response

Submitted solely to this journal?

Yes

Has there been a previous version?	No
Do you or any of your co-authors have a conflict of interest to declare?	No. The authors declare no conflict of interest.

Spatially-Controlled Occlusion of Polymer-Stabilized Gold Nanoparticles within ZnO

Yin Ning,* Lee A. Fielding, Alexander N. Kulak, Fiona C. Meldrum, and Steven P. Armes*

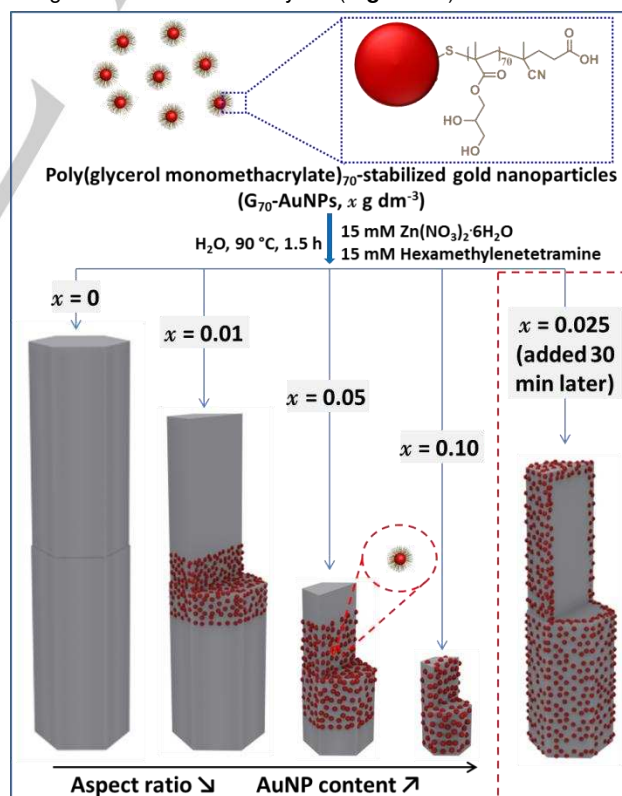
Abstract: In principle, incorporating nanoparticles into growing crystals offers an attractive and highly convenient route for the production of a wide range of novel nanocomposites. Herein we describe an efficient aqueous route that enables the *spatially-controlled* occlusion of gold nanoparticles (AuNPs) within growing ZnO crystals at up to 20 % by mass. Depending on the precise synthesis protocol, these AuNPs can be (i) solely located within a central region, (ii) uniformly distributed throughout the ZnO host crystal or (iii) confined to a surface layer. Remarkably, such efficient occlusion is mediated by a *non-ionic* water-soluble polymer, poly(glycerol monomethacrylate)₇₀ (G₇₀), which is chemically grafted to the AuNPs; pendent *cis*-diol side-groups on this steric stabilizer bind Zn²⁺ cations, which promotes nanoparticle interaction with the growing ZnO crystals. Finally, *uniform* occlusion of G₇₀-AuNPs within this inorganic host leads to faster UV-induced photodegradation of a model dye.

Biominerals provide many wonderful examples of the incorporation of water-soluble biomacromolecules within various inorganic crystals, such as bones, teeth and seashells.^[1] However, incorporating *nanoparticles* into inorganic crystals is much more challenging.^[2] This is because crystallization normally favors impurity expulsion, rather than occlusion.^[3] Nevertheless, various inorganic nanoparticles (e.g. Pt, Au, Fe₃O₄, quantum dots, etc) have been encapsulated into zeolites,^[4] metal-organic frameworks (MOFs),^[5] and ionic crystals,^[6] albeit typically at relatively low loadings. In related work, inorganic nanoparticles can also be incorporated into CaCO₃ (calcite)^[7] or Cu₂O^[8] respectively using a gel-trapping or confinement-based strategy.

There is a growing number of literature reports describing the occlusion of various *anionic* nanoparticles with appropriate surface functionality (such as carboxylate,^[9] sulfonate^[10] or sulfate groups^[11]) within *single* crystals (e.g. calcite or ZnO). Such wholly synthetic systems provide a new approach for the preparation of new nanocomposite crystals, while enabling the convenient introduction of color,^[7a, 9c] magnetism,^[7a, 10a] fluorescence^[6] or enhanced mechanical properties (e.g. hardness).^[9a, 9b, 9f] However, good control over the *spatial distribution* of guest nanoparticles within growing host inorganic crystals has not yet been achieved.

Herein we report efficient, spatially-controlled occlusion of

non-ionic poly(glycerol monomethacrylate)₇₀-stabilized gold nanoparticles (G₇₀-AuNPs; see supporting information for further synthesis and characterization details, **Figures S1-S4**) within ZnO crystals generated in aqueous solution (**Scheme 1**). It is emphasized that this occlusion strategy differentiates our work from the many literature examples of Au/ZnO nanocomposites in which AuNPs are merely adsorbed at the surface of ZnO crystals.^[12] Serendipitously, we found that G₇₀-AuNPs were efficiently incorporated within ZnO crystals generated by heating an aqueous solution containing Zn(NO₃)₂·6H₂O and hexamethylenetetramine at 90 °C for 1.5 h. In the absence of any G₇₀-AuNPs, twinned ZnO rods were obtained (**Figure 1a**). In the presence of 0.01 g dm⁻³ G₇₀-AuNPs (Au core diameter = 4.8 nm), nanoparticle occlusion was mainly confined to the central region of the ZnO rods, as indicated by the bracket shown in **Figure 1b**. [In addition, larger G₇₀-AuNPs (Au core diameter = 14 nm) were also prepared to aid nanoparticle imaging within the central region of the ZnO rods via SEM, see **Figure S5**]. Using a higher concentration of 4.8 nm G₇₀-AuNPs (0.05 g dm⁻³) led to a larger central zone (**Figure 1c**, see brackets) and, when utilized at 0.075 g dm⁻³, essentially all the G₇₀-AuNPs are more or less uniformly distributed throughout the ZnO crystals (**Figure S6**). At 0.10 g dm⁻³, the G₇₀-AuNPs are uniformly distributed throughout the whole ZnO crystal (**Figure 1d**).



Scheme 1. Schematic representation of spatially-controlled occlusion of poly(glycerol monomethacrylate)₇₀-stabilized gold nanoparticles (G₇₀-AuNPs) within ZnO crystals. A twin-structured ZnO rod-like crystal is obtained in the absence of any G₇₀-AuNPs ($x = 0$), whereas the other four sectioned rods indicate the spatial distribution of G₇₀-AuNPs both inside the ZnO crystal ($x = 0.01$ to 0.10) and also confined to a 35 nm surface layer ($x = 0.025$).

[a] Dr. Y. Ning, Prof. S. P. Armes
Department of Chemistry, University of Sheffield, Brook Hill,
Sheffield, South Yorkshire S3 7HF, UK.
E-mail: Y.Ning@sheffield.ac.uk; s.p.armes@sheffield.ac.uk

[b] Dr. L. A. Fielding
The School of Materials, University of Manchester, Oxford Road,
Manchester, M13 9PL, UK.

[c] Dr. A. N. Kulak, Prof. F. C. Meldrum
School of Chemistry, University of Leeds, Woodhouse Lane, Leeds,
LS2 9JT, UK.

Supporting information for this article is given via a link at the end of the document. ((Please delete this text if not appropriate))

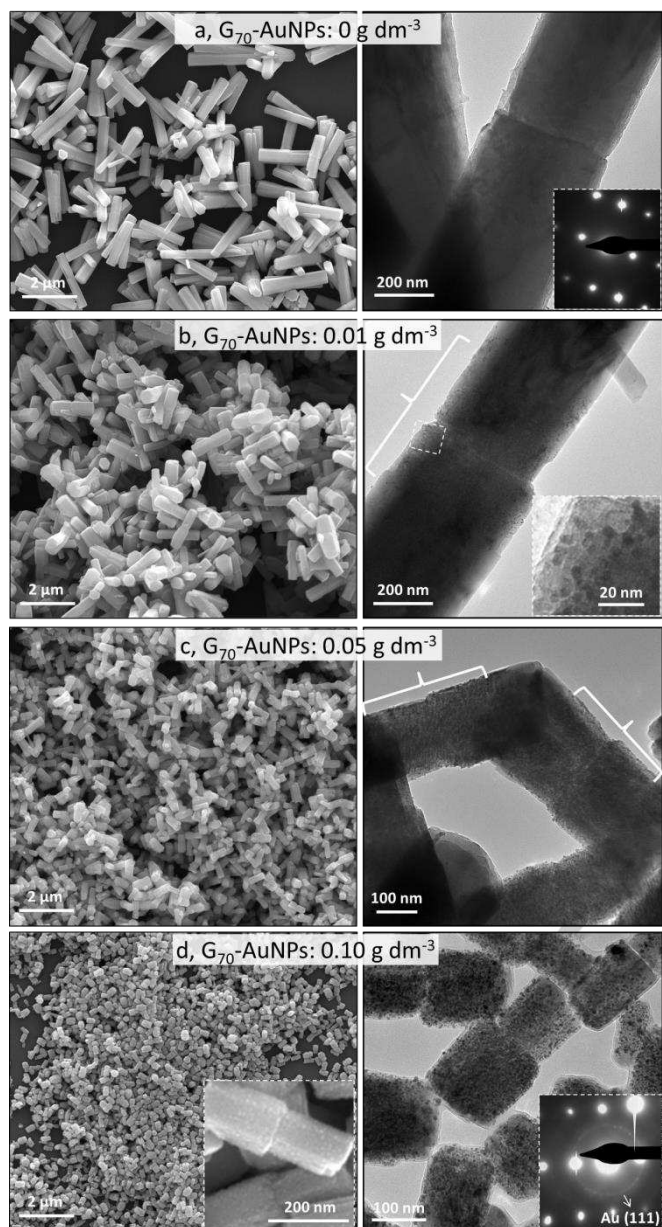


Figure 1. SEM images (left column) and TEM images (right column) obtained for ZnO crystals prepared in the presence of various concentrations (x) of G_{70} -AuNPs. (a), $x = 0 \text{ g dm}^{-3}$ G_{70} -AuNPs (pure ZnO control); (b) $x = 0.01 \text{ g dm}^{-3}$; (c), $x = 0.05 \text{ g dm}^{-3}$; (d), $x = 0.10 \text{ g dm}^{-3}$; The insets in (a) and (d) in the TEM images represent selected-area electron diffraction (SAED) patterns recorded for each corresponding sample. The inset shown in (b) is a higher magnification TEM image of the indicated region. The left inset in (d) is a higher magnification SEM image showing ZnO rods surface-decorated with gold nanoparticles (see white dots). The right inset in (d) shows the corresponding SAED pattern, indicating the single crystal nature of these ZnO particles and also a ring of diffraction spots assigned to the Au (111) planes. The brackets shown in (b) and (c) indicate the spatial location of the AuNPs within the central region of the ZnO rods.

High-resolution TEM images recorded for ultramicrotomed G_{70} -Au/ZnO nanocomposite crystals embedded in epoxy resin confirmed that the G_{70} -AuNPs were incorporated within the host matrix, rather than merely being deposited on its surface (Figure 2). By imaging the cross-section parallel to the c axis of the ZnO

crystals (Figures 2a~2e), G_{70} -AuNPs (which appear darker than the host crystal owing to their higher electron density) are clearly preferentially located within the central core of the ZnO rods when used at a relatively low concentration of 0.05 g dm^{-3} (denoted as G_{70} -Au(central)/ZnO, Figures 2a~2c). In contrast, a uniform distribution of AuNPs throughout the ZnO crystal was achieved at 0.10 g dm^{-3} (denoted as G_{70} -Au(uniform)/ZnO, Figures 2d~2e). The spatial distribution of AuNPs was further examined by imaging cross-sections made perpendicular to the c axis of the G_{70} -Au/ZnO rods (Figures 2f~2k). In a control experiment, ultramicrotomed ZnO crystals prepared in the absence of any AuNPs exhibited the expected hexagonal shape (Figure 2f).^[13] When using 0.10 g dm^{-3} G_{70} -AuNPs, G_{70} -AuNPs were homogeneously occluded throughout the ZnO rods (Figure 2g). At this point, we hypothesized that ZnO crystals might also be prepared in which G_{70} -AuNPs are solely located within a surface layer. This objective was achieved via delayed addition of the G_{70} -AuNPs during ZnO formation. Under such conditions, ultramicrotomed cross-sections indicate that G_{70} -AuNPs are mainly confined to a $\sim 35 \text{ nm}$ surface layer within the ZnO crystal (denoted as G_{70} -Au(surface)/ZnO), as shown in Figures 2j and 2k. As indicated in Figures 2e, 2h and 2i, characteristic ZnO lattice fringes can be clearly observed, suggesting that AuNP occlusion does not disrupt the host crystal. Further high magnification TEM images are shown in Figures S7-S8. Selected area electron diffraction (SAED) patterns obtained for the ZnO control (Figure 1a) confirmed its single crystal nature, with additional ring of diffraction spots corresponding to AuNPs being observed for the G_{70} -Au(uniform)/ZnO nanocomposite crystals (Figure 1d). Powder XRD studies confirmed that all of the ZnO particles had the wurtzite structure, whether they were prepared in the presence or absence of G_{70} -AuNPs (Figure S9).

Given the presence of the G_{70} stabilizer chains at the surface of the AuNPs, it is perhaps surprising that no distinct interfacial region is observed between the AuNPs and the ZnO matrix (Figures 2e, 2h and 2i). However, the surface density of the G_{70} chains on the AuNPs is calculated using Equation S1 (see Supporting Information) to be approximately $0.54 \text{ chains nm}^{-2}$, which is relatively low.^[14] Hence ZnO crystal growth can penetrate within the G_{70} stabilizer layer, leading to intimate contact with the AuNP cores. This was confirmed by XPS studies, which indicate a charge transfer interaction between Au and ZnO (Figure S10). In this context, it is perhaps noteworthy that Asenath-Smith et al.^[8b] also reported intimate contact between guest citrate-stabilized AuNPs and host Cu_2O crystals. Furthermore, Kulak et al.^[10] did not observe any interfacial host-guest region for block copolymer-stabilized magnetite sols occluded within either calcite or ZnO.

The extent of occlusion of the G_{70} -AuNPs within ZnO increased when using higher G_{70} -AuNP concentrations, as determined by inductively-coupled plasma mass spectrometry (ICP-MS, Table S1). Remarkably, ZnO crystals containing up to 11.9 % gold by mass (or 19.9 % G_{70} -AuNPs by mass) can be prepared under uniform occlusion conditions, e.g. when using 0.10 g dm^{-3} G_{70} -AuNPs. Clearly, the G_{70} stabilizer chains play a key role in the interaction between the AuNPs and the growing host crystal. At first sight this seems rather counter-intuitive because the *non-ionic* nature of poly(glycerol monomethacrylate) might be expected to produce little or no

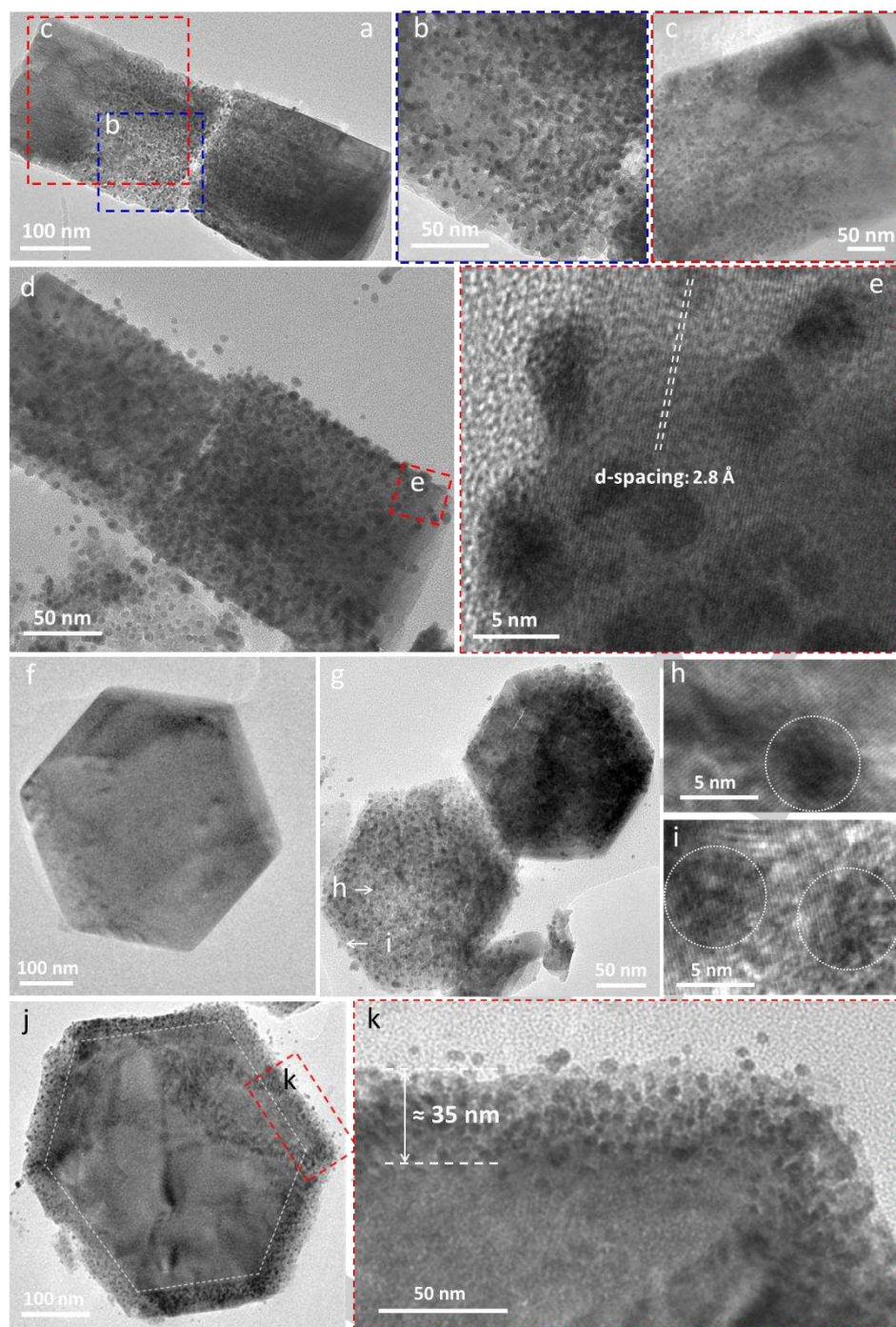


Figure 2. TEM images of ultramicrotomed cross-sections of G_{70} -Au/ZnO nanocomposite crystals with (a)~(e): parallel to the c axis and (f)~(k): perpendicular to the c axis. (a-c) $0.05 \text{ g dm}^{-3} G_{70}\text{-Au(central)/ZnO}$, with (b) and (c) representing magnified regions, as indicated in (a); (d-e) $0.10 \text{ g dm}^{-3} G_{70}\text{-Au(uniform)/ZnO}$, with (e) again representing magnified regions, as indicated in (d). (f) ZnO control; (g) $0.10 \text{ g dm}^{-3} G_{70}\text{-Au(uniform)/ZnO}$ nanocomposites with uniformly-distributed G_{70} -AuNPs; high magnification images (h) and (i) show the continuity of the crystal lattice, the open circles indicate the AuNPs; (j) $G_{70}\text{-Au(surface)/ZnO}$ with G_{70} -AuNPs occluded within ZnO rod-like crystals in the form of a $\sim 35 \text{ nm}$ surface layer; (k) magnified image of the corresponding area indicated in (j).

interaction with the ZnO lattice. Indeed, previous reports suggest that *anionic* surface charge density is required for efficient interaction of copolymer nanoparticles within calcite or ZnO

crystals.^[9-11] The G_{70} chains used in this study contain a terminal carboxylic acid unit but further experiments confirm that such anionic end-groups are not actually required to achieve efficient occlusion within ZnO (**Figure S11**). So how do the G_{70} -AuNPs interact with the growing ZnO? Bearing in mind a report by Cölfen and co-workers on polyacrylamide interactions with ZnO crystals,^[16] the most likely explanation involves chelation between the Zn^{2+} cations and the *cis*-diol groups on the non-ionic G_{70} stabilizer chains.^[15] Experimental evidence for this complexation is provided by vibrational spectroscopy (**Figure 3a**). In FT-IR spectra recorded for G_{70} -AuNPs and G_{70} homopolymer, the absorption bands at 1255 cm^{-1} and 1275 cm^{-1} are assigned to the in-plane bending vibrations of primary and secondary C-OH, respectively.^[17] These two bands merge to form a single new band at 1264 cm^{-1} for $G_{70}\text{-Au/ZnO}$ nanocomposites, which supports the postulated chelation of Zn^{2+} cations by the G_{70} chains (see inset shown in **Figure 3a** and also **Figure S12** for the control experiment conducted in the presence of a stoichiometric amount of $\text{Zn}(\text{NO}_3)_2$).^[18]

Compared to the ZnO control, the mean length and width of the $G_{70}\text{-Au/ZnO}$ nanocomposite crystals are systematically reduced when grown in the presence of higher concentrations of $G_{70}\text{-AuNPs}$ (**Figure 3b**). More specifically, the mean length is dramatically reduced relative to the mean width, resulting in a much lower aspect ratio for the anisotropic ZnO crystals. This indicates that $G_{70}\text{-AuNPs}$ bind preferentially to the polar (0001) face relative to the six non-polar $\{10\bar{1}0\}$ faces, thereby retarding the crystal growth rate and producing less anisotropic ZnO rods (see Supporting Information for more detailed discussion).^[9a] At a relatively low $G_{70}\text{-AuNP}$ concentration (i.e. $< 0.05 \text{ g dm}^{-3}$), nanoparticle occlusion is complete

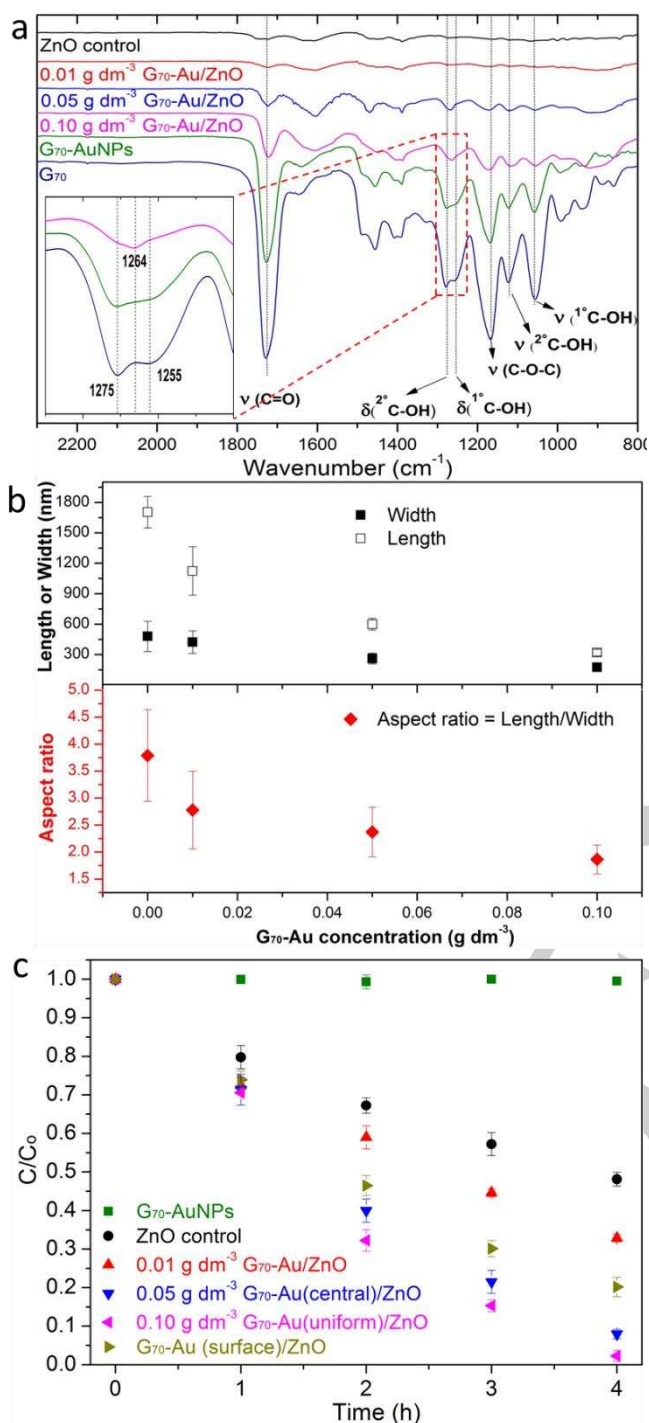


Figure 3. (a) FT-IR spectra recorded for three G₇₀-Au/ZnO nanocomposite crystals and three reference materials (ZnO crystals alone, G₇₀ homopolymer and the G₇₀-AuNPs); (b) Length, width and aspect ratio of G₇₀-Au/ZnO versus G₇₀-AuNP concentration; (c) UV photocatalytic decomposition rates observed at 20 °C and pH 7 (6 W source, λ = 254 nm) for a model rhodamine B dye in the presence of three G₇₀-Au/ZnO nanocomposite crystals and two control samples.

before ZnO crystallization has ceased, leading to G₇₀-AuNPs being confined within a central region. At higher G₇₀-AuNP concentrations, there are sufficient G₇₀-AuNPs present to

become occluded throughout the host crystal, while ZnO growth is significantly retarded.

Finally, we briefly explored the photocatalytic properties of these Au/ZnO nanocomposite crystals with different spatial distribution of AuNPs. Preliminary data confirm that the rate of UV photodegradation of a model rhodamine B dye increases monotonically with their AuNP content (**Figure 3c**). More importantly, the catalytic efficiency obtained for G₇₀-Au(uniform)/ZnO significantly exceeds that of G₇₀-Au(surface)/ZnO, which suggests that uniform occlusion of G₇₀-AuNPs *within* ZnO is required for optimal catalytic performance (see control experiments in **Figure S13** and further discussion in the Supporting Information).

In summary, we report an efficient, versatile and scalable route to incorporate sterically-stabilized gold nanoparticles within ZnO single crystals. This study provides the first example of nanoparticle occlusion within inorganic crystals with *well-controlled spatial distribution* as well as tunable extent of occlusion, which offers an unprecedented opportunity to elucidate synthesis-structure-property relationships. We show for the first time that a *non-ionic* polymer stabilizer can promote highly efficient nanoparticle occlusion into inorganic host crystals. This represents an important paradigm shift because almost all prior literature reports in this area utilize *anionic* polymers as steric stabilizers. We rationalize the occlusion mechanism in terms of Zn²⁺ complexation to the non-ionic stabilizer chains and demonstrate that incorporation of AuNPs into ZnO crystals enhances their photocatalytic performance. In principle, appropriate surface modification of various other metal nanoparticles should enable their efficient occlusion within ZnO (and perhaps other host crystals), thus providing access to a range of new functional nanocomposite materials that are likely to exhibit emergent properties. We intend to explore this concept in the near future.

Acknowledgements

The Overseas Study Program of Guangzhou Elite Project and EPSRC (EP/P005241/1) are acknowledged for PhD sponsorship and post-doctoral support of Y.N., respectively. We thank EPSRC for post-doctoral support (EP/J018589/1 and EP/K006290/1) and SPA acknowledges a five-year ERC Advanced Investigator grant (PISA 320372). We thank Prof. G. J. Leggett and Dr. D. Hammond for useful XPS discussion, Prof. B. Inkson and Dr. S. Tzokov for TEM assistance and Dr. C. Hill for ultramicrotomy.

Keywords: spatially-controlled occlusion • metal/semiconductor nanocomposites • gold nanoparticles • ZnO • RAFT polymerization

- [1] a) A. Berman, L. Addadi, S. Weiner, *Nature* **1988**, *331*, 546-548; b) A. Berman, L. Addadi, A. Kvik, L. Leiserowitz, M. Nelson, S. Weiner, *Science* **1990**, *250*, 664-667; c) A. M. Belcher, X. H. Wu, R. J. Christensen, P. K. Hansma, G. D. Stucky, D. E. Morse, *Nature* **1996**, *381*, 56-58; d) E. Weber, B. Pokroy, *CrystEngComm* **2015**, *17*, 5873-5883; e) S. Mann, *Biomaterialization, Principles and Concepts in*

- 1 *Bioinorganic Materials Chemistry*; Oxford University Press: Oxford,
2 **2001**; f) H. A. Lowenstam, S. Weiner, *On biomineralization*, Oxford
3 University Press, **1989**, 207-251; g) S. Mann, D. D. Archibald, J. M.
4 Didymus, T. Douglas, B. R. Heywood, F. C. Meldrum, N. J. Reeves,
5 *Science* **1993**, *261*, 1286-1292; h) F. C. Meldrum, H. Cölfen, *Chem.*
6 *Rev.* **2008**, *108*, 4332-4432; i) A.-W. Xu, Y. Ma, H. Cölfen, *J. Mater.*
7 *Chem.* **2007**, *17*, 415-449.
- [2] a) J. D. Pasteris, J. J. Freeman, B. Wopenka, K. Qi, Q. Ma, K. L.
8 Wooley, *Astrobiology* **2006**, *6*, 625-643; b) C. H. Lu, L. M. Qi, H. L.
9 Cong, X. Y. Wang, J. H. Yang, L. L. Yang, D. Y. Zhang, J. M. Ma, W. X.
10 Cao, *Chem. Mater.* **2005**, *17*, 5218-5224; c) A. Hanisch, P. Yang, A. N.
11 Kulak, L. A. Fielding, F. C. Meldrum, S. P. Armes, *Macromolecules*
12 **2016**, *49*, 192-204; d) H. Li, H. L. Xin, D. A. Muller, L. A. Estroff,
13 *Science* **2009**, *326*, 1244-1247.
- [3] B. Kahr, R. W. Gurney, *Chem. Rev.* **2001**, *101*, 893-951.
- [4] N. Wang, Q. Sun, R. Bai, X. Li, G. Guo, J. Yu, *J. Am. Chem. Soc.* **2016**,
15 *138*, 7484-7487.
- [5] G. Lu, S. Li, Z. Guo, O. K. Farha, B. G. Hauser, X. Qi, Y. Wang, X.
16 Wang, S. Han, X. Liu, *Nat. Chem.* **2012**, *4*, 310-316.
- [6] a) M. Müller, M. Kaiser, G. M. Stachowski, U. Resch-Genger, N.
17 Gaponik, A. Eychmüller, *Chem. Mater.* **2014**, *26*, 3231-3237; b) T. Otto,
18 M. Müller, P. Munda, V. Lesnyak, H. V. Demir, N. Gaponik, A.
19 Eychmüller, *Nano Lett.* **2012**, *12*, 5348-5354.
- [7] a) Y. Liu, W. Yuan, Y. Shi, X. Chen, Y. Wang, H. Chen, H. Li, *Angew.*
20 *Chem. Int. Ed.* **2014**, *53*, 4127-4131; b) Y. Liu, H. Zang, L. Wang, W.
21 Fu, W. Yuan, J. Wu, X. Jin, J. Han, C. Wu, Y. Wang, H. L. Xin, H. Chen,
22 H. Li, *Chem. Mater.* **2016**, *28*, 7537-7543.
- [8] a) A. E. DiCorato, E. Asenath-Smith, A. N. Kulak, F. C. Meldrum, L. A.
23 Estroff, *Cryst. Growth & Des.* **2016**, *16*, 6804-6811; b) E. Asenath-
24 Smith, J. M. Noble, R. Hovden, A. M. Uhl, A. DiCorato, Y.-Y. Kim, A. N.
25 Kulak, F. C. Meldrum, L. F. Kourkoutis, L. A. Estroff, *Chem. Mater.*
26 **2017**, *29*, 555-563.
- [9] a) Y.-Y. Kim, L. Ribeiro, F. Maillot, O. Ward, S. J. Eichhorn, F. C.
27 Meldrum, *Adv. Mater.* **2010**, *22*, 2082-2086; b) Y.-Y. Kim, K. Ganesan,
28 P. Yang, A. N. Kulak, S. Borukhin, S. Pechook, L. Ribeiro, R. Kroeger,
29 S. J. Eichhorn, S. P. Armes, B. Pokroy, F. C. Meldrum, *Nat. Mater.*
30 **2011**, *10*, 890-896; c) A. N. Kulak, P. Yang, Y.-Y. Kim, S. P. Armes, F.
31 C. Meldrum, *Chem. Commun.* **2014**, *50*, 67-69; d) K. Rae Cho, Y.-Y.
32 Kim, P. Yang, W. Cai, H. Pan, A. N. Kulak, J. L. Lau, P. Kulshreshtha,
33 S. P. Armes, F. C. Meldrum, J. J. De Yoreo, *Nat. Commun.* **2016**, *7*,
34 10187; e) Y. Ning, L. A. Fielding, K. E. B. Doncom, N. J. W. Penfold, A.
35 N. Kulak, H. Matsuoka, S. P. Armes, *ACS Macro Lett.* **2016**, *5*, 311-
36 315; f) Y.-Y. Kim, M. Semsarilar, J. D. Carloni, K. R. Cho, A. N. Kulak, I.
37 Polishchuk, C. T. Hendley, P. J. M. Smeets, L. A. Fielding, B. Pokroy, C.
38 C. Tang, L. A. Estroff, S. P. Baker, S. P. Armes, F. C. Meldrum, *Adv.*
39 *Funct. Mater.* **2016**, *26*, 1382-1392; g) R. Muñoz-Espí, Y. Qi, I.
40 Lieberwirth, C. M. Gómez, G. Wegner, *Chem. Eur. J.* **2006**, *12*, 118-
41 129.
- [10] a) A. N. Kulak, M. Semsarilar, Y.-Y. Kim, J. Ihli, L. A. Fielding, O.
42 Cespedes, S. P. Armes, F. C. Meldrum, *Chemical Science* **2014**, *5*,
43 738-743; b) A. N. Kulak, R. Grimes, Y.-Y. Kim, M. Semsarilar, C.
44 Anduix-Canto, O. Cespedes, S. P. Armes, F. C. Meldrum, *Chem. Mater.*
45 **2016**, *28*, 7528-7536.
- [11] a) Y. Ning, L. A. Fielding, T. S. Andrews, D. J. Gowney, S. P. Armes,
46 *Nanoscale* **2015**, *7*, 6691-6702; b) Y. Ning, L. A. Fielding, L. P. D.
47 Ratcliffe, Y.-W. Wang, F. C. Meldrum, S. P. Armes, *J. Am. Chem. Soc.*
48 **2016**, *138*, 11734-11742.
- [12] a) W. He, H.-K. Kim, W. G. Wamer, D. Melka, J. H. Callahan, J.-J. Yin,
49 *J. Am. Chem. Soc.* **2013**, *136*, 750-757; b) X. Liu, M.-H. Liu, Y.-C. Luo,
50 C.-Y. Mou, S. D. Lin, H. Cheng, J.-M. Chen, J.-F. Lee, T.-S. Lin, *J. Am.*
51 *Chem. Soc.* **2012**, *134*, 10251-10258; c) M. Murdoch, G. I. N.
52 Waterhouse, M. A. Nadeem, J. B. Metson, M. A. Keane, R. F. Howe, J.
53 Llorca, H. Idriss, *Nat. Chem.* **2011**, *3*, 489-492; d) F. Xiao, F. Wang, X.
54 Fu, Y. Zheng, *J. Mater. Chem.* **2012**, *22*, 2868-2877; e) J. Lee, H. S.
55 Shim, M. Lee, J. K. Song, D. Lee, *J. Phys. Chem. Lett.* **2011**, *2*, 2840-
56 2845; f) R. Jiang, B. Li, C. Fang, J. Wang, *Adv. Mater.* **2014**, *26*, 5274-
57 5309; g) S. T. Kochuveedu, J. H. Oh, Y. R. Do, D. H. Kim, *Chem. Eur. J.*
58 **2012**, *18*, 7467-7472; h) Y. H. Jang, S. Y. Yang, Y. J. Jang, C. Park, J.
59 K. Kim, D. H. Kim, *Chem. Eur. J.* **2011**, *17*, 2068-2076.
- [13] Z. L. Wang, *J. Phys. Condens. Matter.* **2004**, *16*, R829-R858.
- [14] M. Liang, I. C. Lin, M. R. Whittaker, R. F. Minchin, M. J. Monteiro, I.
60 Toth, *ACS Nano* **2010**, *4*, 403-413.
- [15] a) S. P. Kawatkar, D. A. Kuntz, R. J. Woods, D. R. Rose, G.-J. Boons, *J.*
61 *Am. Chem. Soc.* **2006**, *128*, 8310-8319; b) B. Gyurcsik, L. Nagy, *Coord.*
62 *Chem. Rev.* **2000**, *203*, 81-149; c) T. Ghoshal, S. Kar, S. Chaudhuri,
63 *Cryst. Growth & Des.* **2007**, *7*, 136-141.
- [16] Y. Peng, A.-W. Xu, B. Deng, M. Antonietti, H. Cölfen, *J. Phys. Chem. B*
64 **2006**, *110*, 2988-2993.
- [17] G. Socrates, *Infrared and Raman characteristic group frequencies:
65 tables and charts*, John Wiley & Sons, **2004**.
- [18] N. J. Richards, D. G. Williams, *Carbohydr. Res.* **1970**, *12*, 409-420.

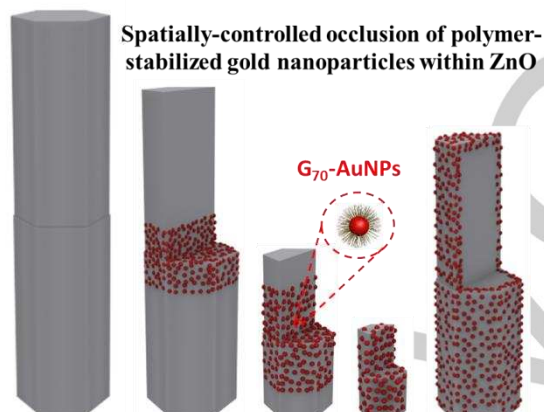
1 **Entry for the Table of Contents** (Please choose one layout)
2
3

4 Layout 1:
5
6

7 **COMMUNICATION**
8

9 **Spatially-controlled occlusion**
10 **of non-ionic poly(glycerol**
11 **monomethacrylate)₇₀-**
12 **stabilized gold nanoparticles**
13 **(G₇₀-AuNPs) within ZnO**

14 **crystals** can be achieved at
15 remarkably high levels (up to
16 ~20 % by mass) during *in situ*
17 growth of ZnO crystals in
18 aqueous solution. This study
19 reports a straightforward yet
20 efficient route for the *localized*
21 occlusion of nanoparticles into
22



Yin Ning,* Lee A. Fielding,
Alexander N. Kulak, Fiona C.
Meldrum, and Steven P.
Armes*

Page No. – Page No.

**Spatially-Controlled
Occlusion of Polymer-
Stabilized Gold
Nanoparticles within ZnO**

1
2
3
4
5
6
7 Supporting Information
8 ©Wiley-VCH 2016
9
10 69451 Weinheim, Germany
11
12
13
14

15 **Spatially-Controlled Occlusion of Polymer-Stabilized Gold Nanoparticles**
16 **within ZnO**
17

18
19 Yin Ning,* Lee A. Fielding, Alexander N. Kulak, Fiona C. Meldrum, and Steven P. Armes*
20
21
22
23
24
25
26
27
28
29
30
31
32
33
34
35
36
37
38
39
40
41
42
43
44

45
46 **DOI: 10.1002/anie.2016XXXXX**
47
48
49
50
51
52
53
54
55
56
57
58
59
60
61
62
63
64
65

Experimental section

Chemicals

Glycerol monomethacrylate (GMA; 99.8%) was donated by GEO Specialty Chemicals (Hythe, UK) and used without further purification. 4-Cyano-4 (phenylcarbonothioylthio)pentanoic acid (CPCP), 2-cyano-2-propyl benzodithioate (CPB), 2,2'-azobis(isobutylnitrile) (AIBN) 4,4'-azobis(4-cyanovaleic acid) (ACVA), zinc nitrate hexahydrate, hexamethylenetetramine (HMTA), rhodamine B (RhB), sodium citrate tribasic dihydrate, sodium borohydride and gold(III) chloride trihydrate ($\text{HAuCl}_4 \cdot 3\text{H}_2\text{O}$) were all purchased from Sigma-Aldrich (UK) and used as received. Deionized water was obtained from an Elgastat Option 3A water purification unit.

Synthesis of poly(glycerol monomethacrylate)₇₀ [G₇₀] homopolymer

To a round-bottomed flask containing CPCP RAFT agent (0.96 g, 3.43 mmol), GMA monomer (38.44 g, 0.24 mol) and anhydrous ethanol (59.40 g, 1.28 mol) was added to afford a target degree of polymerization (DP) of 70. ACVA initiator (0.19 g, 0.69 mmol, CTA/ACVA molar ratio = 5.0) was then added to this pink solution, which was sparged with N_2 for 20 min before immersing the sealed flask into an oil bath set at 70 °C. After 2.5 h, the polymerization was quenched by immersing the flask in an ice bath and exposing its contents to air. The polymerization solution was then precipitated into a ten-fold excess of dichloromethane and washed three times with this solvent before being placed under high vacuum for three days at 40 °C. ^1H NMR analysis indicated a mean DP of 70. Taking into account the target DP of 70 and the conversion of 85 %, this suggests a CTA efficiency of 85 %. DMF GPC analysis (vs. a series of near-monodisperse poly(methyl methacrylate) calibration standards) indicated M_n and M_w/M_n values of 17,000 g mol^{-1} and 1.10, respectively.

Synthesis of poly(glycerol monomethacrylate)₇₀-stabilized gold nanoparticles (G₇₀-AuNPs)

The synthesis of gold nanoparticles has previously been reported elsewhere^[1]. In the present study, 480 mL deionized water was charged into a 1000 mL beaker and then 5.0 mL of 10 g dm^{-3} gold(III) chloride trihydrate was added and stirred for 5 minutes. Thereafter, an aqueous solution of sodium citrate (10 mL, 38.8 mM) was added and stirred for another 5 min before rapid addition of an aqueous solution of sodium borohydride (5.0 mL, 0.075 % w/w), containing sodium citrate tribasic dehydrate (57 mg, 38.8 mM). G₇₀ homopolymer (100 mg) was dissolved in 10 mL deionized water and added to

1 the gold sol. Excess G₇₀ homopolymer and sodium citrate were removed by centrifugation, followed by
2 dialysis against deionized water for 7 days, using dialysis tubing with a molecular weight cut-off of 50
3 kD.
4

5
6 For the 14 nm gold nanoparticles, 500 mL deionized water was mixed with 30.0 mL 1 % w/w sodium
7 citrate solution in a 1000 mL beaker and boiled for 5 min, followed by the rapid addition of 5.0 mL of a
8 10 g dm⁻³ aqueous solution of gold(III) chloride trihydrate. The reaction was allowed to proceed for 15
9 min. 100 mg G₇₀ homopolymer dissolved in 10.0 mL water was then added and the resulting G₇₀-
10 modified gold nanoparticles were purified by multiple centrifugation-redispersion cycles, with
11 successive supernatants being replaced with deionized water.
12
13
14
15
16
17

21 **Synthesis of G₇₀-Au/ZnO nanocomposite crystal**

22
23 Aqueous G₇₀-AuNP dispersions (0.50 g dm⁻³, 2.0 – 30.0 mL) were added to a two-necked flask
24 containing 96.0 – 68.0 ml of an aqueous solution of zinc nitrate hexahydrate (0.446 g, 1.50 mmol) to
25 give a total volume of 98.0 mL. This flask was connected to a condenser and transferred to a preheated
26 oil bath set at 90 °C and the reaction mixture was magnetically stirred to achieve thermal equilibrium
27 (typically 30 min). ZnO formation was commenced on slow addition of 2.0 mL of an aqueous solution
28 of HMTA (0.210 g, 1.50 mmol). The reaction was quenched after 90 minutes by cooling in an ice-water
29 bath. The precipitate was isolated by centrifugation and washed several times using water or ethanol,
30 followed by drying under vacuum at 40 °C. For surface-confined G₇₀-Au NP occlusion, G₇₀-AuNPs
31 were added to the same reaction solution after 30 min, rather than at the beginning of the reaction.
32
33
34
35
36
37
38
39
40
41
42

43 **Photocatalytic degradation of RhB using UV irradiation**

44
45
46 G₇₀-Au/ZnO nanocomposites (10 mg) were dispersed in deionized water (18.0 mL) with the aid of an
47 ultrasonic bath for 10 minutes. 2.0 mL of a 1.0 × 10⁻⁴ M RhB stock solution was added and
48 continuously stirred in the dark for 30 min before irradiation using a UV lamp (6 W, peak emission =
49 254 nm). Aliquots were extracted at various times and centrifuged prior to recording the visible
50 absorption spectrum of the supernatant solution. The photodegradation of the RhB dye was monitored
51 via gradual reduction in its absorption maximum at 553 nm. Photocatalysis experiment was conducted
52 at pH 7 under room temperature (20 °C) and repeated in triplicate.
53
54
55
56
57
58
59
60
61
62
63
64
65

Characterization

¹H NMR spectroscopy

¹H NMR spectra were recorded using a Bruker Avance 400 spectrometer operating at 400 MHz using CD₃OD as the solvent.

Gel permeation chromatography (GPC)

The DMF GPC instrument comprised two Polymer Laboratories PL gel 5 mm Mixed C columns, one PL polar gel 5 mm guard column connected in series to a Varian 390-LC multi-detector suite (refractive index detector only), a Varian 290-LC pump injection module and was operated at 60 °C. The GPC eluent was HPLC grade DMF containing 10 mM LiBr and was filtered prior to use. The flow rate used was 1.0 mL min⁻¹ and DMSO was used as a flow-rate marker. Calibration was conducted using a series of ten near-monodisperse poly(methyl methacrylate) standards ($M_n = 6.25 \times 10^2 - 6.18 \times 10^5$ g mol⁻¹, $K = 2.094 \times 10^{-3}$, $\alpha = 0.642$).

Dynamic light scattering (DLS)

DLS measurements were conducted using a Malvern Zetasizer NanoZS instrument by detecting back-scattered light at an angle of 173°. The concentration of aqueous dispersions of various gold nanoparticles with or without 15 mM zinc ions were fixed at 0.05 g dm⁻³.

Transmission electron microscopy (TEM)

TEM specimens of gold nanoparticles or G₇₀-Au/ZnO nanocomposites were prepared by adsorbing the samples onto carbon film coated palladium-copper grids, which were treated with a plasma glow discharge for about 30 seconds to create a hydrophilic surface prior to addition of the aqueous sample dispersion (5 µL). Excess solvent was removed via blotting and the grid was carefully dried under vacuum. To examine internal structures, the G₇₀-Au/ZnO nanocomposites were embedded in Araldite resin mixture and cured at 60 °C for 48-72 h. Ultrathin sections, approximately 85 nm in thickness, were cut using a Leica UC 6 ultramicrotomy equipped with a Diatome diamond knife onto 200 mesh copper grids. TEM images were performed using either a FEI Tecnai G2 Spirit instrument (120 kV) or a high resolution TEM (Philips FEG-CM200) operating at an accelerating voltage of 200 kV.

Scanning electron microscopy (SEM)

The nanocomposite morphologies were investigated using scanning electron microscopy (either a FEI Nova NanoSEM 450 or FEI Inspect F). The specimens were prepared by dropping Au-G₇₀/ZnO aqueous dispersion onto a cleaned glass slide and dried at room temperature. All the samples were iridium-coated before imaging.

X-ray photoelectron spectroscopy (XPS)

XPS samples were prepared by adding a drop of nanocomposite aqueous dispersion onto clean indium foil and left overnight at room temperature. The powder samples were directly pressed on a clean indium foil. The instrument used to collect the XPS data was a Kratos Axis Ultra DLD equipped with a monochromatic Al X-ray radiation at 6.0 mA and 15 kV at a typical base pressure of 10⁻⁸ Torr. The step size was 0.5 eV for the survey spectra (pass energy = 160 eV) and 0.05 eV for the high resolution spectra (pass energy = 20 eV). The raw data was corrected by a transmission function characteristic of the instrument, determined using software from the National Physical Laboratory. The adjusted data was then quantified using the theoretically derived Scofield relative sensitivity factors.

Other measurements

FT-IR spectra were recorded on KBr pellets using a Nicolet 7199 FT-IR spectrometer. Thermogravimetric analysis (TGA) was conducted using a Perkin-Elmer Pyris 1 TGA instrument under air atmosphere from 20 °C to 900 °C at a heating rate of 15 °C min⁻¹. The elemental analysis was conducted using a Perkin Elmer 2400 Series II CHNS/O Elemental Analyser. Powder X-ray diffraction (XRD) measurements were made using a Bruker D2 Phaser Desktop X-ray diffractometer equipped with Ni-filtered Cu K α radiation ($\lambda = 1.542 \text{ \AA}$) operating at an accelerating voltage and emission current of 30 kV and 10 mA, respectively. The Au content of G₇₀-Au/ZnO nanocomposite particles was determined by a Hewlett-Packard 4500 inductively-coupled plasma mass spectrometry (ICP-MS, Hewlett-Packard, Yokogawa Corporation, Japan). UV-visible spectra were recorded at 20 °C for the nanocomposite aqueous dispersion using a Perkin-Elmer Lambda 25 instrument operating between 200 and 800 nm. Specific surface areas were determined via BET surface area analysis using N₂ as an adsorbate at 77 K. The densities of the G₇₀-Au and G₇₀-Au/ZnO nanocomposites were determined by

helium pycnometry at 20 °C (Micrometrics AccuPyc 1330 helium pycnometer). The number-average mean diameter of the Au nanoparticles was determined by analyzing TEM images (more than 200 AuNPs) using ImageJ software.

1
2
3
4
5
6
7
8
9
10
11
12
13
14
15
16
17
18
19
20
21
22
23
24
25
26
27
28
29
30
31
32
33
34
35
36
37
38
39
40
41
42
43
44
45
46
47
48
49
50
51
52
53
54
55
56
57
58
59
60
61
62
63
64
65

Calculation of surface density of G₇₀ homopolymer chains on Au NPs using Equation S1

Based on thermogravimetric analysis data, the weight percentage of G₇₀ homopolymer (W_p) can be obtained and the weight percentage of the Au cores is readily calculated by difference (see below).

Assuming the mass of G₇₀-Au is m , then the mass of G₇₀ is given by $m \times W_p$, and the mass of Au is $m \times (100 - W_p)$.

Hence the number of G₇₀ polymer chains = $\frac{mW_p}{M_p} N_A$, where M_p is the molecular weight of G₇₀.

The number of Au nanoparticles = $\frac{m(100-W_p)}{\frac{4}{3}\pi\rho r^3}$

Total surface area of Au nanoparticles = $\frac{m(100-W_p)}{\frac{4}{3}\pi\rho r^3} \times 4\pi r^2$

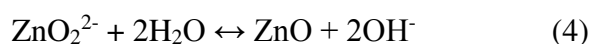
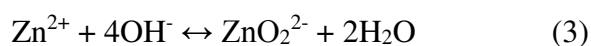
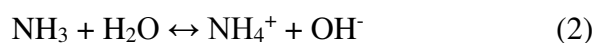
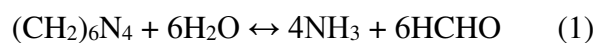
Thus the surface density of G₇₀ homopolymer chains = $\left(\frac{W_p}{100-W_p}\right) \times \frac{r\rho N_A}{3M_p} = \left(\frac{40}{100-40}\right) \times$

$$\frac{2.4 \text{ nm} \times 19.3 \text{ g cm}^{-3} \times 6.02 \times 10^{23} \text{ mol}^{-1}}{3 \times 11491 \text{ g mol}^{-1}} = 0.54 \text{ chains nm}^{-2}$$

Occlusion mechanism

1
2 It is well-known that hexagonal ZnO crystals possess polar (0001) and (000 $\bar{1}$) planes, with the former
3
4 being rich in zinc atoms while the latter is rich in oxygen atoms.^[2] The relative growth velocity, V , of
5
6 each plane follows the order $V_{[0001]} > V_{[10\bar{1}0]} > V_{[000\bar{1}]}$. This explains why elongated rod-like ZnO crystals
7
8 are formed, as shown in Figure 1a. In this study, HMTA is used to generate hydroxide anions via a
9
10 hydrolysis reaction that produces formaldehyde and ammonia (see reaction scheme shown below).^[3]
11
12
13

14 The four main reactions involved in the formation of ZnO crystals are as follows:
15
16
17



31 In the early stages of ZnO crystallization, anionic ZnO_2^{2-} units (the ZnO growth unit under weakly
32
33 acidic conditions) are preferentially absorbed onto cationic (0001) faces.^[3b] Meanwhile, HMTA
34
35 hydrolyzes and forms the cationic (fully protonated) $(\text{CH}_2)_6\text{N}_4\text{-}4\text{H}^+$ complex in aqueous solution,^[4]
36
37 which interacts with the (000 $\bar{1}$) face via coulombic interaction.^[3b] Moreover, this cationic complex also
38
39 interacts with the ZnO_2^{2-} precursor species.^[3] This leads to the formation of ZnO crystals on the (000 $\bar{1}$)
40
41 surface. Thus, a twinned structure with a common basal plane and 180° reversed polarity is gradually
42
43
44
45
46 formed via preferential growth in two opposing directions.^[3]
47
48
49
50
51
52
53
54
55
56
57
58
59
60
61
62
63
64
65

Synthesis and Characterization of G₇₀-AuNPs.

1
2 Poly(glycerol monomethacrylate)₇₀ (see Figure S1a) was synthesized via reversible addition-
3
4 fragmentation chain transfer (RAFT) polymerization in ethanol using 4-cyano-4-
5
6 (phenylcarbonothioylthio)pentanoic acid (CPCP) and 4,4'-azobis(4-cyanovaleric acid) as RAFT chain
7
8 transfer agent and initiator, respectively. This water-soluble G₇₀ homopolymer contains dithiobenzoate
9
10 transfer agent and initiator, respectively. This water-soluble G₇₀ homopolymer contains dithiobenzoate
11
12 and carboxylic acid end-groups and possesses a narrow molecular weight distribution ($M_n = 17\,000\text{ g}$
13
14 mol^{-1} , $M_w/M_n = 1.10$), as confirmed by gel permeation chromatography (GPC, see Figure S1b). An
15
16 aqueous dispersion of AuNPs was prepared as described elsewhere.^[1] G₇₀-AuNPs were prepared via
17
18 chemisorption conducted in aqueous solution; the dithiobenzoate terminal group on the G₇₀ chains is
19
20 known to bind strongly to gold surfaces.^[5] As shown in Figures S1c and S1d, the as-synthesized G₇₀-
21
22 AuNPs had a mean TEM diameter of $4.8 \pm 0.9\text{ nm}$. It is well-known that the surface plasmon band of
23
24 AuNPs of a given size is sensitive to their surface modification.^[6] Indeed, the surface plasmon band was
25
26 red-shifted by 4 nm after surface-grafting the G₇₀ chains (see inset in Figure S1e). This chemical
27
28 modification led to a subtle change in color from pink to purple for the AuNP dispersion (see Figure S2).
29
30 According to dynamic light scattering (DLS, see Figure S3) studies, the mean hydrodynamic diameters
31
32 of the citrate-stabilized AuNPs and G₇₀-AuNPs were $6.4 \pm 1.6\text{ nm}$ and $11.5 \pm 2.8\text{ nm}$, respectively. This
33
34 difference indicates a G₇₀ stabilizer layer thickness of $\sim 2.5\text{ nm}$, which is consistent with recent small-
35
36 angle X-ray scattering studies.^[7] Thermogravimetric analyses (TGA, see Figure S4) indicated that the
37
38 G₇₀ stabilizer comprised approximately 40% by mass of the G₇₀-AuNPs. This composition was
39
40 corroborated by carbon microanalyses, which indicated a G₇₀ content of $\sim 41\%$.
41
42
43
44
45
46
47

48 The original citrate-stabilized AuNPs aggregate immediately in the presence of zinc ions (see Figures
49
50 S2 and S3). This salt-induced coagulation is corroborated by the disappearance of the surface plasmon
51
52 absorbance (see Figure S1e) and the observation of $\sim 700\text{ nm}$ aggregates by DLS (see Figure S3). In
53
54 contrast, the surface plasmon band observed for G₇₀-AuNPs remains unchanged in the presence of zinc
55
56 ions (Figure S1e). More specifically, G₇₀-AuNPs retain their colloidal stability in the presence of 15
57
58
59
60
61
62
63
64
65

mM $\text{Zn}(\text{NO}_3)_2$, which is an essential prerequisite for their subsequent efficient occlusion within ZnO crystals.

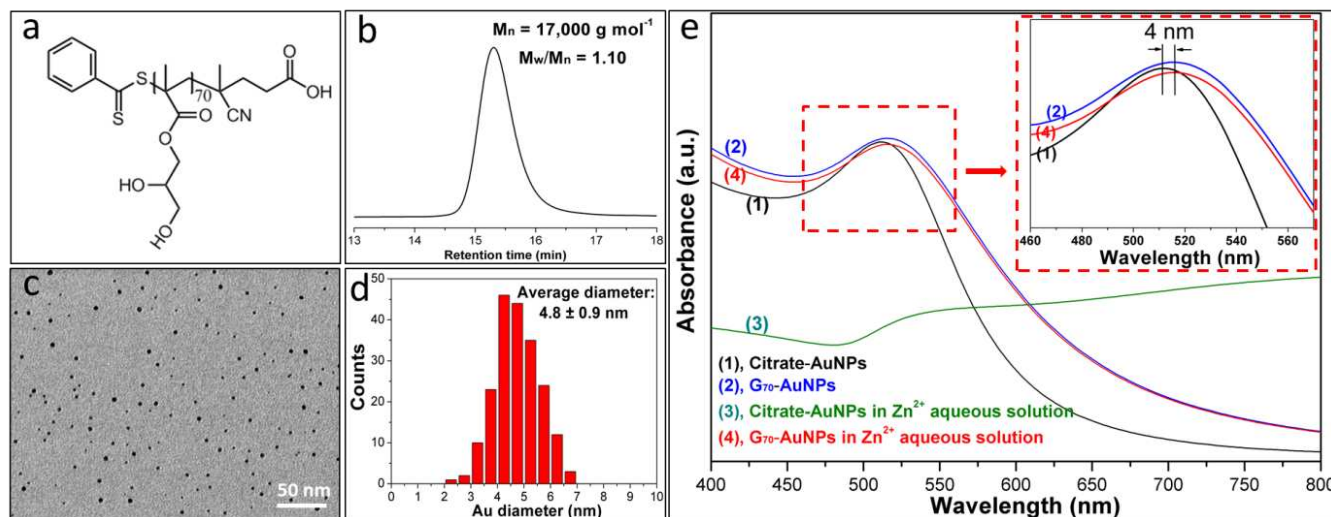


Figure S1. Characterization of poly(glycerol monomethacrylate)₇₀ (G_{70}) and G_{70} -stabilized AuNPs. (a) Chemical structure of the G_{70} polymer; (b) GPC data obtained for G_{70} using a series of poly(methyl methacrylate) calibration standards; (c) representative TEM image obtained for G_{70} -AuNPs; (d) particle size distribution determined for G_{70} -AuNPs from TEM image analysis; (e) Visible absorption spectra recorded for as-synthesized citrate-AuNPs or G_{70} -AuNPs in either water or an aqueous solution of 15 mM $\text{Zn}(\text{NO}_3)_2$. The inset shows that the surface plasmon band for G_{70} -AuNPs is red-shifted by 4 nm compared to citrate-AuNPs. Notably, there is no further change in the presence of 15 mM zinc ions, indicating good colloidal stability for the G_{70} -AuNPs under these conditions.

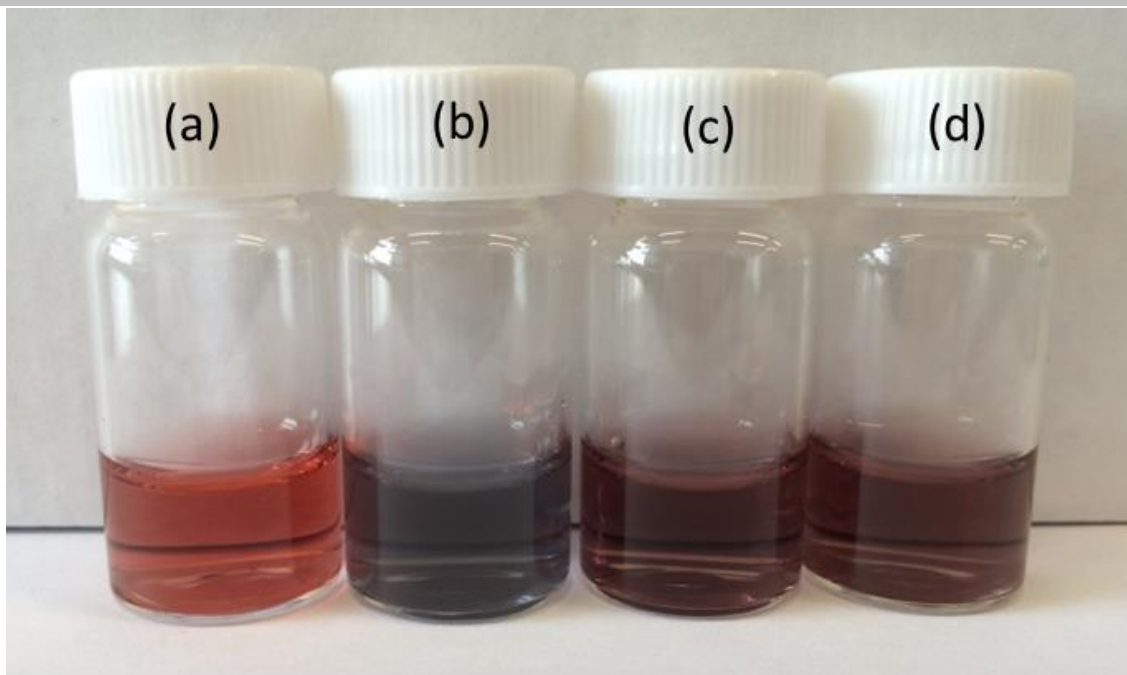


Figure S2. Optical photograph of aqueous dispersions of (a) citrate-stabilized AuNPs (gold nanoparticles prepared using sodium citrate); (b) citrate-stabilized AuNPs in the presence of 15 mM zinc ions; (c) G₇₀-AuNPs; (d) G₇₀-AuNPs in the presence of 15 mM zinc ions. Note: the color of citrate-stabilized AuNPs aqueous solution immediately changed from pink to grey once upon the addition of zinc ions derive from zinc nitrate hexahydrate. This is due to the aggregation of the gold nanoparticle caused by the presence of zinc ions. The aggregation was confirmed by DLS measurements (see **Figure S3**). It is emphasized that there is no discernible colour change between (c) and (d), indicating excellent colloidal stability for the G₇₀-AuNPs even in the presence of zinc ions.

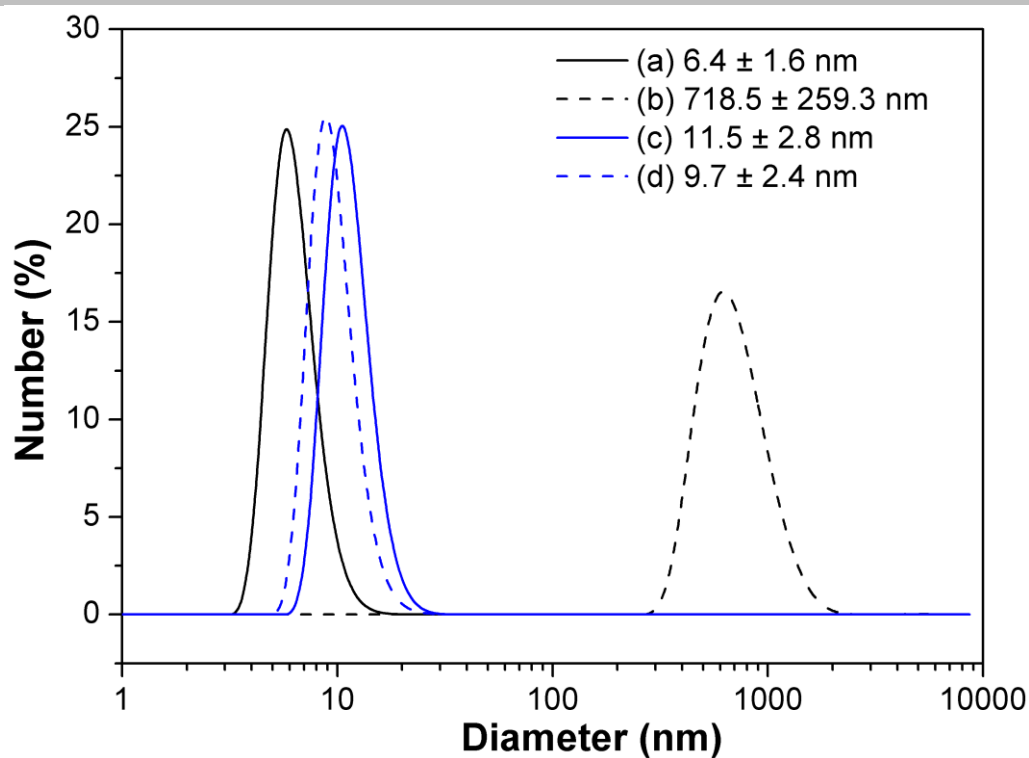


Figure S3. Mean hydrodynamic number-average diameter obtained for (a) citrate-stabilized AuNPs in aqueous solution, (b) citrate-stabilized AuNPs in aqueous solution containing 15 mM $\text{Zn}(\text{NO}_3)_2$, (c) G_{70} -AuNPs in aqueous solution and (d) G_{70} -AuNPs in aqueous solution containing 15 mM $\text{Zn}(\text{NO}_3)_2$.

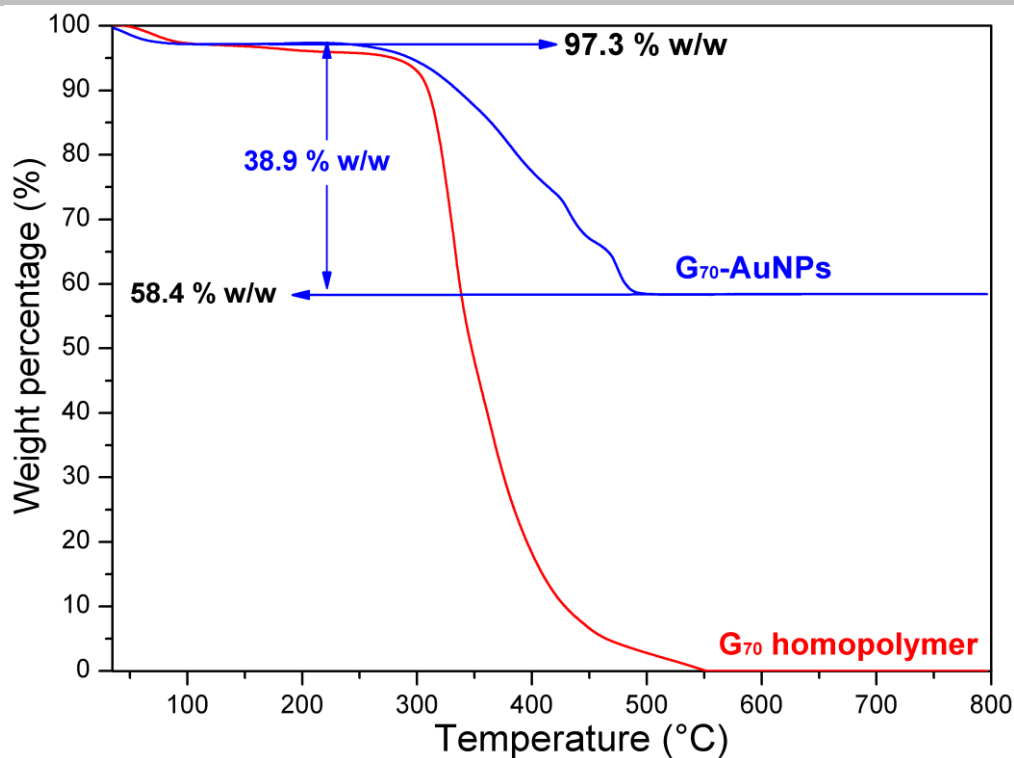


Figure S4. Thermogravimetric analysis (TGA) of G₇₀ homopolymer (red) and G₇₀-AuNPs (blue). As expected, G₇₀ homopolymer is pyrolysed completely above 550 °C. Given the presence of 2.7 % w/w water in the G₇₀-AuNPs, the G₇₀ content of G₇₀-AuNPs can be calculated to be 40.0 % w/w.

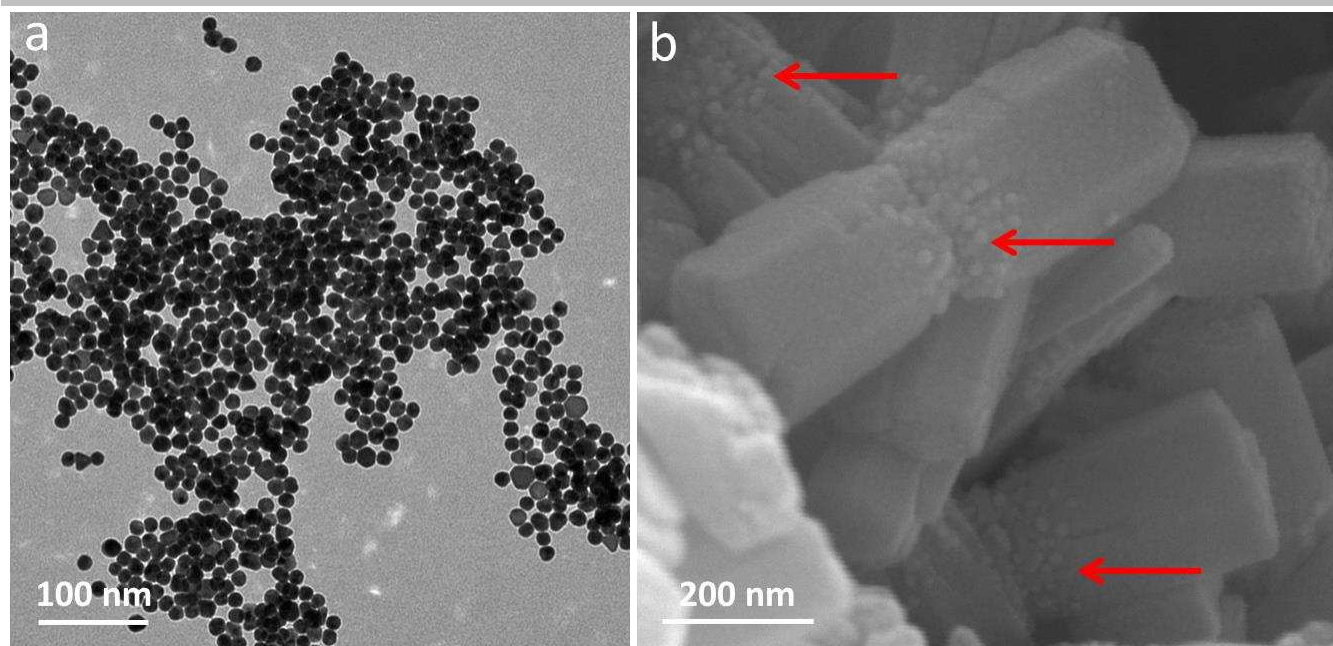
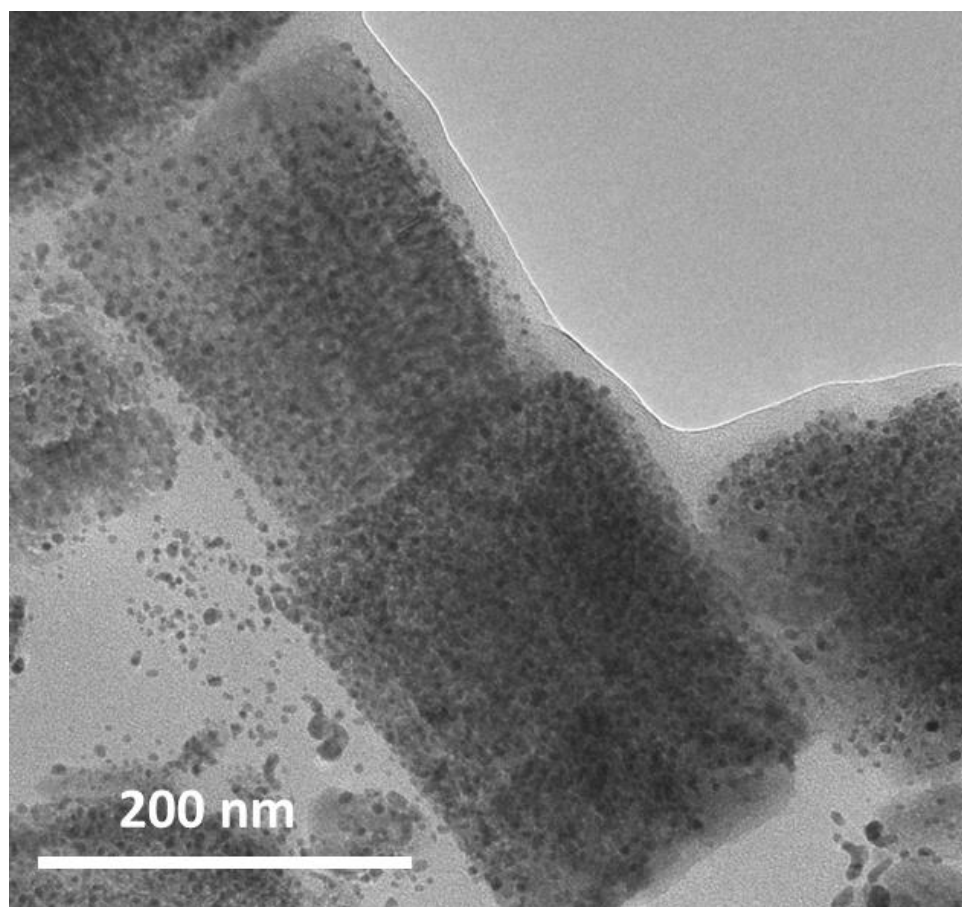


Figure S5. Occlusion of 14 nm G₇₀-AuNPs within ZnO crystals. (a) TEM image recorded for 14 nm G₇₀-AuNPs. (b) SEM image recorded for G₇₀-Au/ZnO nanocomposite crystals prepared using these 14 nm AuNPs. The gold nanoparticles localised in the central region of the rod-like ZnO crystals can be clearly identified, as indicated by the red arrows.



34 **Figure S6.** TEM image recorded for ultramicrotomed cross-section of G₇₀-Au/ZnO nanocomposites
35 prepared in the presence of 0.075 g dm⁻³ G₇₀-AuNPs.
36

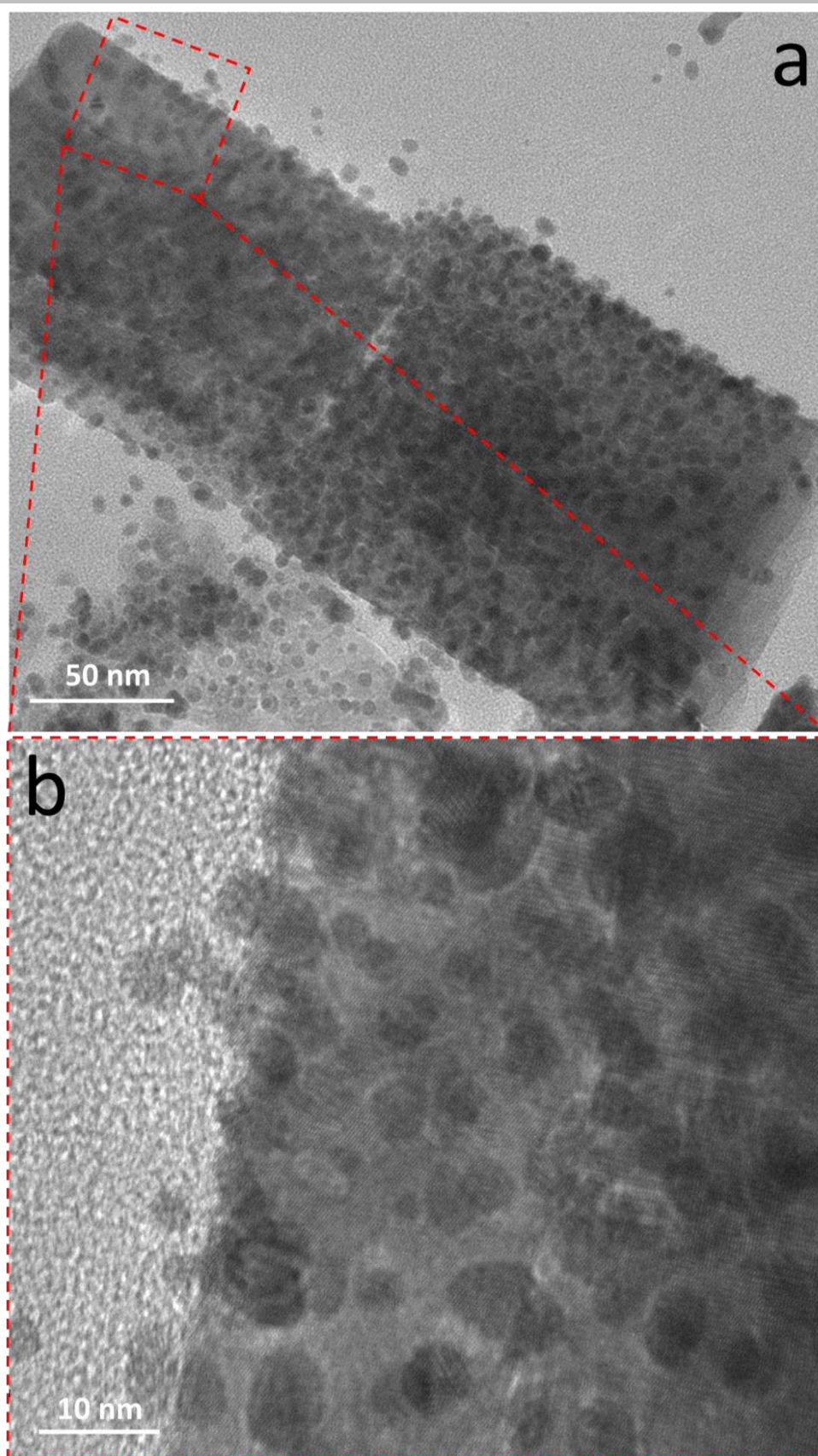


Figure S7. (a) High resolution TEM images of cross-section paralleled to the c -axis. (b) The corresponding magnified area indicated in (a).

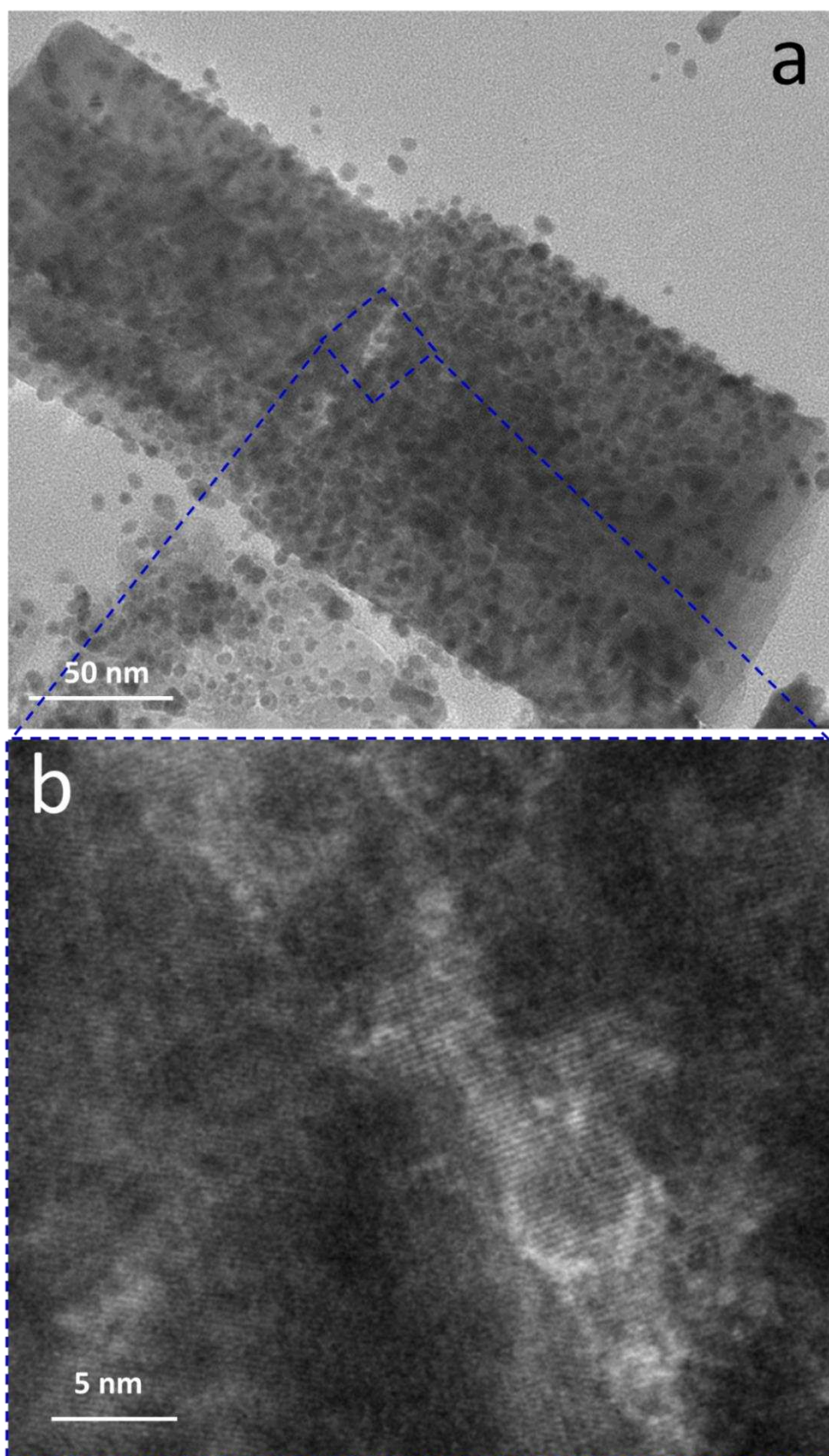


Figure S8. (a) High resolution TEM images of cross-section paralleled to the c -axis. (b) The corresponding magnified area indicated in (a).

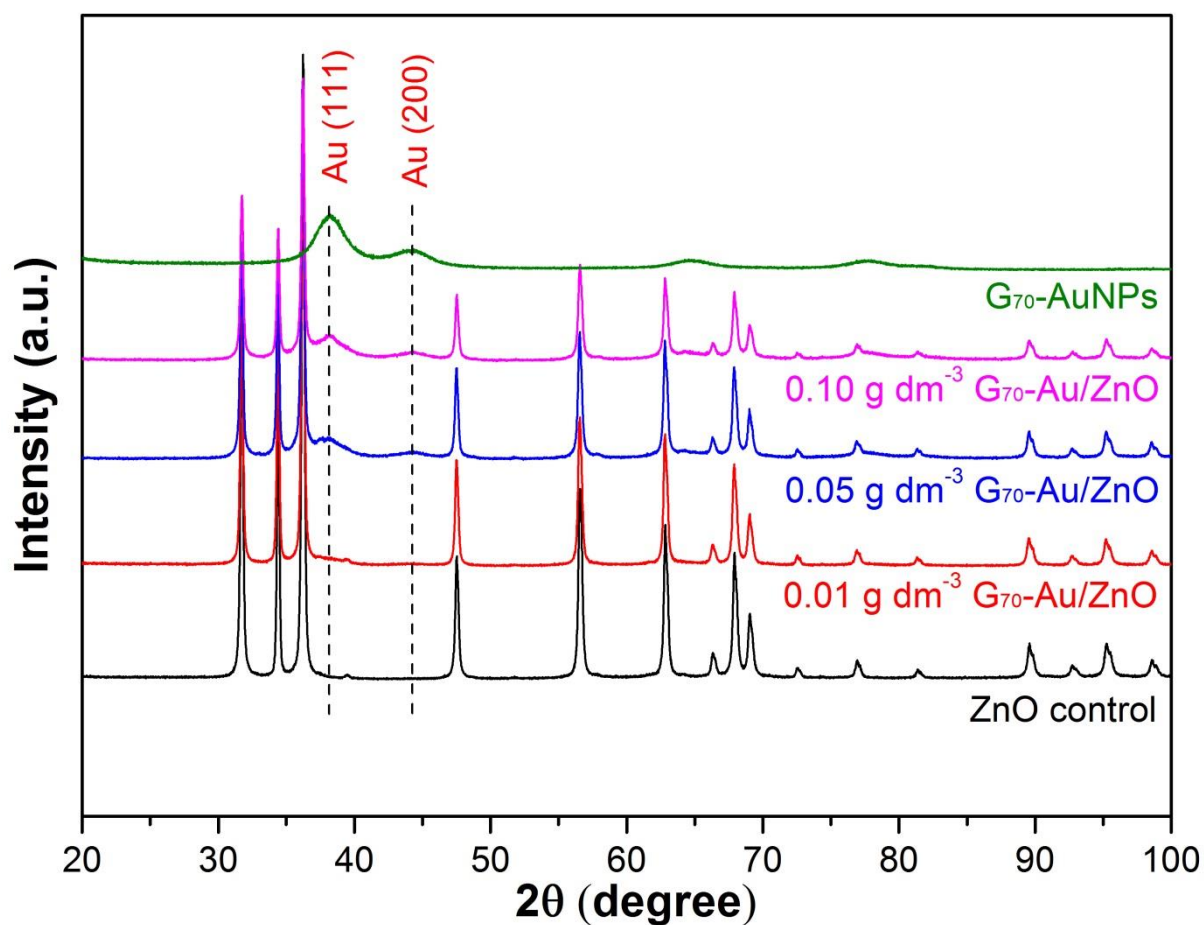


Figure S9. Powder X-ray diffractograms recorded for three examples of G_{70} -Au/ZnO crystals prepared using the stated G_{70} -AuNP concentrations, plus the G_{70} -AuNPs alone and a ZnO control.

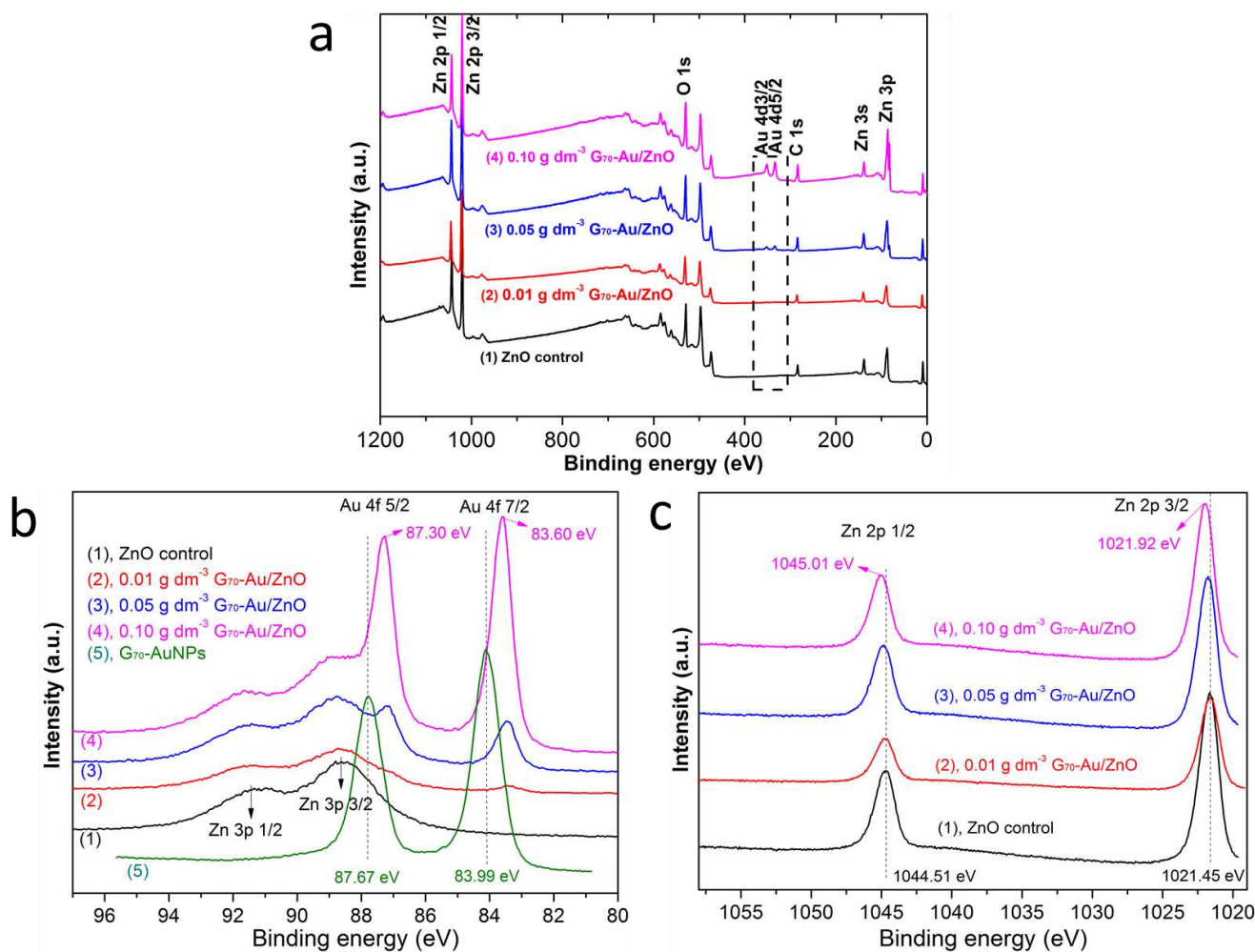


Figure S10. (a) XPS spectra recorded for G_{70} -Au/ZnO nanocomposites prepared at the three stated G_{70} -AuNP concentrations. The Au4d signal intensity systematically increased when using higher G_{70} -AuNP concentrations, as indicated by the black dotted lines. High resolution X-ray photoelectron spectra recorded for various G_{70} -Au/ZnO nanocomposite crystals and appropriate reference materials: (b) Au4f; (c) Zn2p.

The signal intensity of two binding energy (BE) peaks corresponding to the electronic states of Au4f5/2 (87.30 eV) and Au 4f7/2 (83.60 eV) was systematically enhanced at higher AuNP contents. Importantly, each signal was shifted to a lower BE for the G_{70} -Au/ZnO nanocomposite crystals, whereas the two Zn2p signals were shifted to higher BE. These observations suggest significant charge transfer between the two components, indicating an intimate interaction between the AuNPs and the ZnO host crystal.^[8]

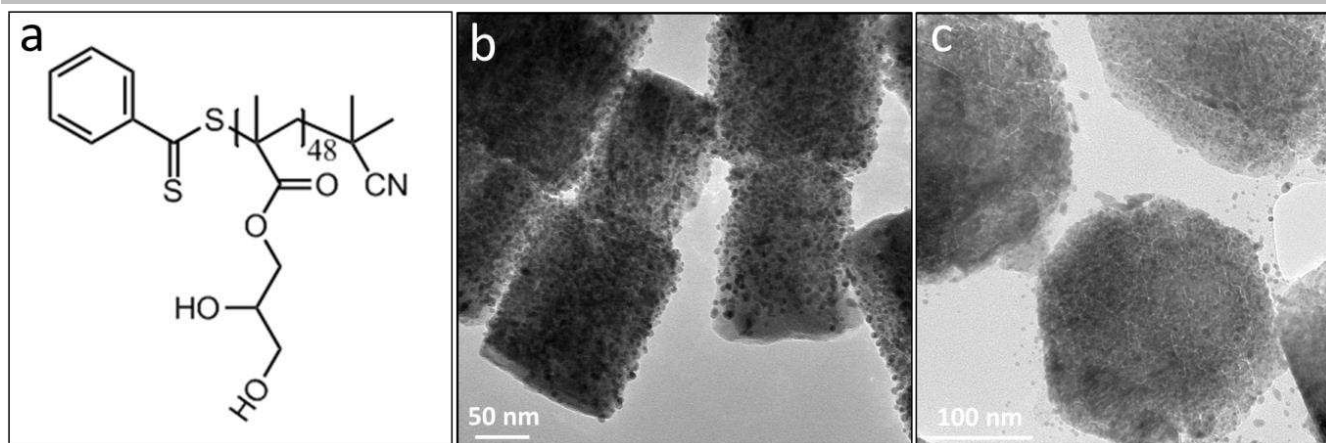


Figure S11. Occlusion of G_{48} -AuNPs (prepared using a poly(glycerol monomethacrylate) $_{48}$ (G_{48}) stabilizer containing no carboxylic acid end-groups) within ZnO crystals. (a) Chemical structure of the G_{48} polymeric stabilizer; (b) TEM image of the as-synthesized G_{48} -Au/ZnO nanocomposite crystal; (c) cross-sectional TEM image obtained for G_{48} -Au/ZnO nanocomposite crystals after ultramicrotomy perpendicular to the c axis. Clearly, G_{48} -AuNPs are uniformly distributed throughout the whole ZnO crystal. For these experiments, G_{48} was prepared via reversible addition-fragmentation chain transfer (RAFT) polymerization in ethanol using 2-cyano-2-propyl benzodithioate (CPB) and 2,2'-azobis(isobutylnitrile) (AIBN) as the RAFT chain transfer agent and initiator, respectively. This synthetic protocol produces G_{48} stabilizer chains with no terminal carboxylic acid unit, which demonstrates that such end-groups are not required for efficient occlusion of G_{48} -AuNPs within ZnO crystals.

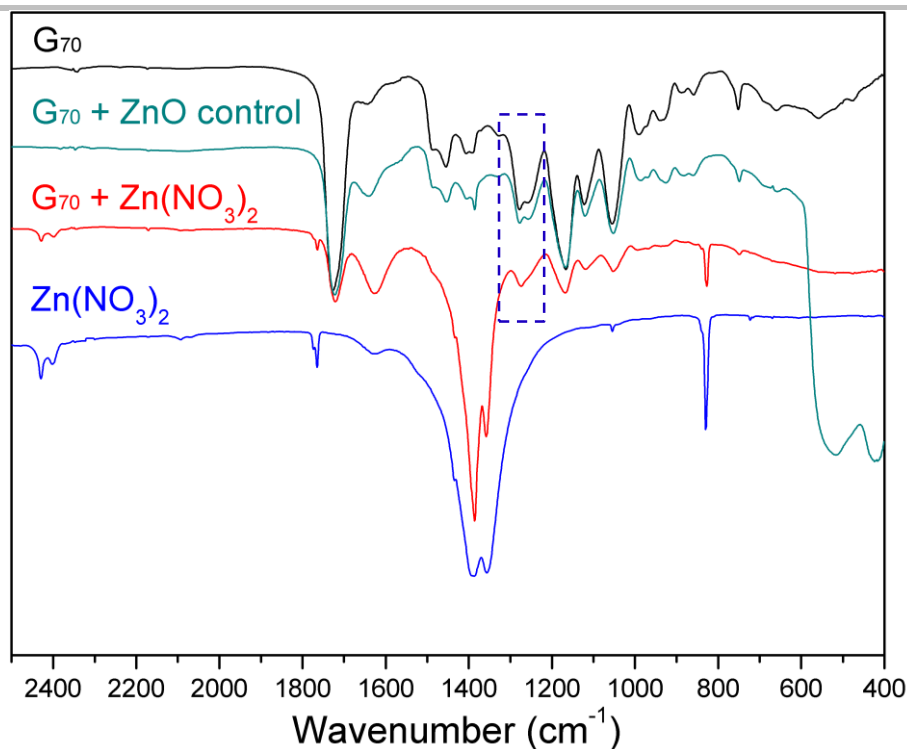


Figure S12. Transmission mode FT-IR spectra recorded for G₇₀, an ad-mixture of G₇₀ plus ZnO, an admixture of G₇₀ plus Zn(NO₃)₂ (prepared by freeze-drying a binary aqueous solution overnight), and Zn(NO₃)₂ alone. Clearly, the G₇₀ plus Zn(NO₃)₂ spectrum is a combination of the G₇₀ and Zn(NO₃)₂ reference spectra, except that the two in-plane bending $\delta_{\text{C-OH}}$ vibrations merge into a single band, as indicated by the dotted blue box. This strongly suggests chelation between Zn²⁺ ions and the *cis*-diol groups on the G₇₀ stabilizer chains, for which there is good literature precedent (see ref. 17 in the main manuscript). Notably, for the G₇₀ plus ZnO control, the $\delta_{\text{C-OH}}$ in-plane bending vibrations remain as two distinct bands, confirming that no interaction occurs on simple physical mixing of these two components.

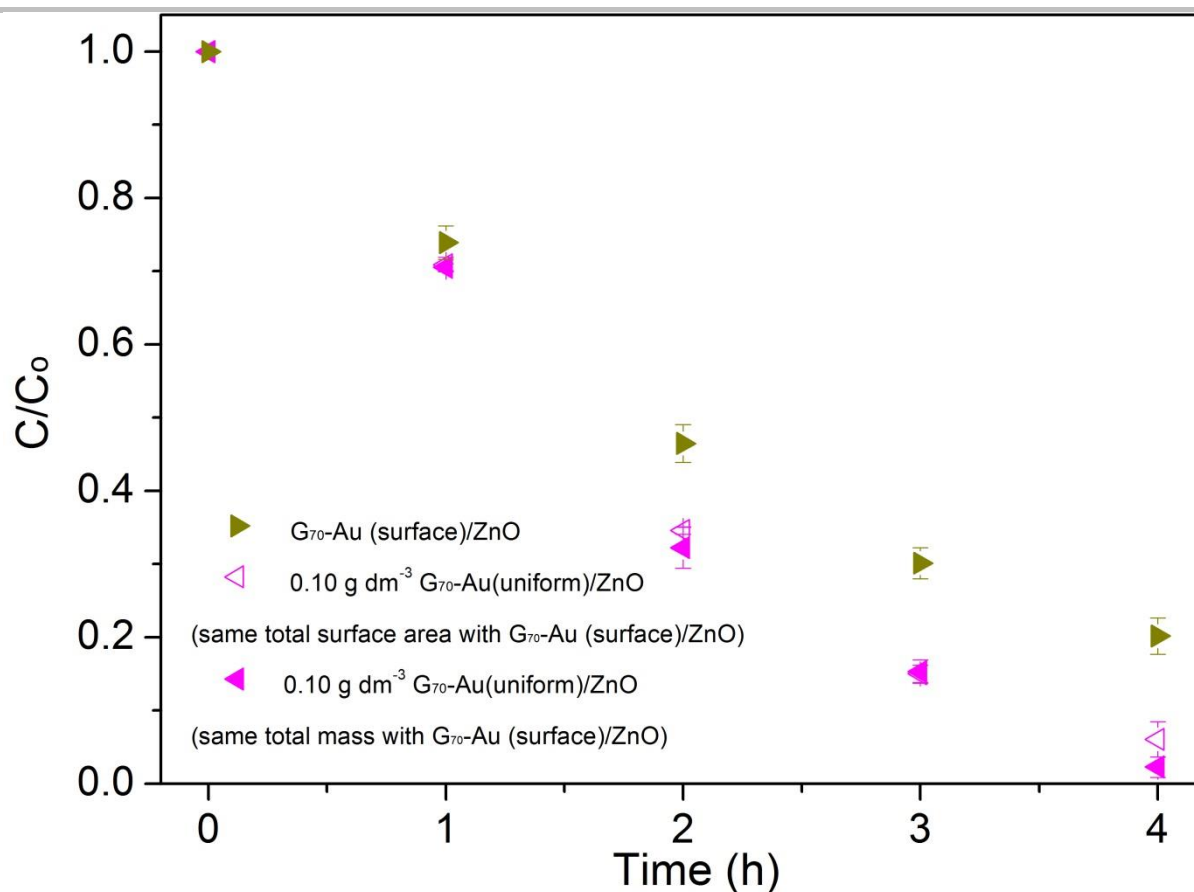


Figure S13. Relative rates of UV-induced photocatalytic decomposition observed for a rhodamine B (RhB) dye in the presence of G₇₀-Au(surface)/ZnO and 0.10 g dm⁻³ G₇₀-Au(uniform)/ZnO. The amount of 0.10 g dm⁻³ G₇₀-Au(uniform)/ZnO crystals used in these experiments was reduced to produce approximately the same total surface area as that for the G₇₀-Au (surface)/ZnO crystals, but this had almost no discernible effect on the rate of dye decomposition.

It is well-known that Au/ZnO nanostructures can exhibit superior photocatalytic performance compared to ZnO alone.^[9] Given that such dye decomposition involves heterogeneous catalysis, the total available surface area could potentially affect photocatalytic performance. However, a control experiment conducted at constant surface area revealed little or no change in the rate of dye decomposition (**Figure S13**). Meanwhile, 0.05 g dm⁻³ G₇₀-Au(central)/ZnO also exhibits a higher catalytic efficiency compared to G₇₀-Au(surface)/ZnO (8.0% vs. 20% dye remains after 4 h). As shown in **Table S1**, 0.05 g dm⁻³ G₇₀-Au(central)/ZnO has approximately twice the Au content compared to G₇₀-Au(surface)/ZnO, but the Au_{4d}/Zn_{2p} surface atomic ratio for the former is around half that of the latter. This observation

1 indicates that the photocatalytic performance mainly depends on the *bulk* Au content, rather than the
2 *surface* Au content. In other words, the incorporated AuNPs contribute significantly to the rate of
3 photocatalysis. This suggests that a higher extent of AuNP occlusion within ZnO provides a larger
4 number of electron ‘sinks’, which facilitate charge carrier separation and extend the lifetime of the
5 electron-hole pair,^[9a, 10] thus producing a more effective photocatalyst.
6
7
8
9
10
11
12
13
14
15
16
17
18
19
20
21
22
23
24
25
26
27
28
29
30
31
32
33
34
35
36
37
38
39
40
41
42
43
44
45
46
47
48
49
50
51
52
53
54
55
56
57
58
59
60
61
62
63
64
65

Table S1. Summary of Au4d/Zn2p atomic ratio (%), solid-state density, BET specific surface area, extent of occlusion of G₇₀-AuNPs within ZnO crystals, and pseudo-first-order rate constant for the UV photodegradation of a model dye (rhodamine B).

Sample	Au4d/Zn2p atomic ratio (%)	Density (g cm ⁻³) ^a	BET surface area (m ² g ⁻¹)	Extent of occlusion (% w/w)				Rate constant (k, h ⁻¹) ^b
				ICP-MS		Helium pycnometry		
				Au	G ₇₀ -Au	Au	G ₇₀ -Au	
ZnO control	0	5.45	4.2 ± 0.2	-	-	-	-	0.18
0.01 g dm ⁻³ G ₇₀ -Au/ZnO	0.9	5.41	3.8 ± 0.3	1.3	2.2	1.1	1.9	0.27
0.05 g dm ⁻³ G ₇₀ -Au/ZnO	7.4	5.22	7.3 ± 0.2	7.0	11.6	6.4	10.7	0.63
0.10 g dm ⁻³ G ₇₀ -Au/ZnO	39.0	5.05	8.4 ± 0.1	11.9	19.9	11.5	19.1	0.84
G ₇₀ -Au (surface)ZnO	15.0	5.31	3.1 ± 0.4	3.4	5.7	3.9	6.4	0.42

^a G₇₀-AuNPs have a density of 3.85 g cm⁻³, therefore the higher the G₇₀-Au content, the lower the density of the nanocomposite crystals.

^b Pseudo-first-order rate constant (k) is derived from $-\ln(C/C_0) = kt$

For helium pycnometry, given the solid-state densities of the ZnO control (5.45 g cm⁻³) and the G₇₀-AuNPs (3.85 g cm⁻³), the G₇₀-AuNP content of these nanocomposite crystals can be determined by measuring their solid-state density via helium pycnometry. These density data are in fairly good agreement with the ICP-MS results.

- [1] G. Frens, *Nature* **1973**, *241*, 20-22.
- [2] Z. L. Wang, *J. Phys. Condens. Matter.* **2004**, *16*, R829-R858.
- [3] a) S. Cho, H. Jeong, D.-H. Park, S.-H. Jung, H.-J. Kim, K.-H. Lee, *CrystEngComm* **2010**, *12*, 968-976; b) Q. Yu, C. Yu, H. Yang, W. Fu, L. Chang, J. Xu, R. Wei, H. Li, H. Zhu, M. Li, G. Zou, G. Wang, C. Shao, Y. Liu, *Inorg. Chem.* **2007**, *46*, 6204-6210.
- [4] H. Tada, *J. Am. Chem. Soc.* **1960**, *82*, 255-263.
- [5] J. W. Hotchkiss, A. B. Lowe, S. G. Boyes, *Chem. Mater.* **2007**, *19*, 6-13.
- [6] a) G. Schneider, G. Decher, *Nano Lett.* **2004**, *4*, 1833-1839; b) Y. Jiang, S. Huo, T. Mizuhara, R. Das, Y.-W. Lee, S. Hou, D. F. Moyano, B. Duncan, X.-J. Liang, V. M. Rotello, *ACS nano* **2015**, *9*, 9986-9993.
- [7] B. F. Akpınar, Lee; Cunningham, Victoria; Ning, Yin; Mykhaylyk, Oleksandr; Fowler, Patrick; Armes, Steven, *Macromolecules* **2016**, *49*, 5160-5171.
- [8] A. E. DiCorato, E. Asenath-Smith, A. N. Kulak, F. C. Meldrum, L. A. Estroff, *Cryst. Growth & Des.* **2016**, *16*, 6804-6811.

[9] a) H. Cui, Z. Chen, S. Zhong, K. L. Wooley, D. J. Pochan, *Science* **2007**, *317*, 647-650; b) P. Li, Z. Wei, T. Wu, Q. Peng, Y. Li, *J. Am. Chem. Soc.* **2011**, *133*, 5660-5663; c) Y. Chen, D. Zeng, K. Zhang, A. Lu, L. Wang, D.-L. Peng, *Nanoscale* **2014**, *6*, 874-881.

[10] S. T. Kochuveedu, Y. H. Jang, D. H. Kim, *Chem. Soc. Rev.* **2013**, *42*, 8467-8493.

1
2
3
4
5
6
7
8
9
10
11
12
13
14
15
16
17
18
19
20
21
22
23
24
25
26
27
28
29
30
31
32
33
34
35
36
37
38
39
40
41
42
43
44
45
46
47
48
49
50
51
52
53
54
55
56
57
58
59
60
61
62
63
64
65